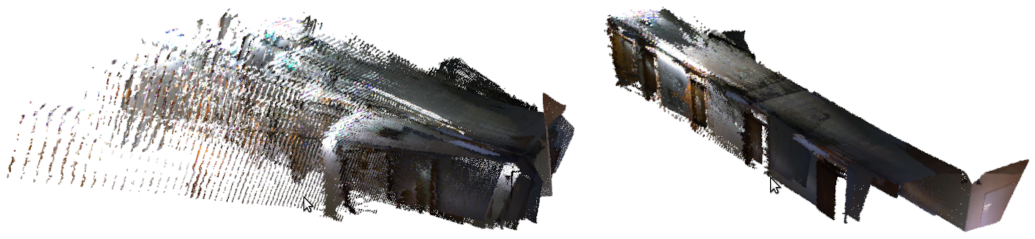

Interactive Mapping Using Range Sensor Data under Localization Uncertainty

Pedro Gonçalo Soares Vieira

Dissertation submitted for obtaining the degree of

Master in Electrical and Computer Engineering

Examination Committee

Chairperson:	Prof. Carlos Filipe Gomes Bispo
Supervisor:	Prof. Rodrigo Martins de Matos Ventura
Member of the committee:	Prof. Carlos António Roque Martinho

December 2012

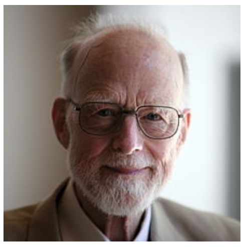

There are two ways of constructing a software design: One way is to make it so simple that there are obviously no deficiencies, and the other way is to make it so complicated that there are no obvious deficiencies. The first method is far more difficult.

Tony Hoare

Acknowledgments

First, I would like express my deepest gratitude and thanks to my thesis supervisor, professor Rodrigo Ventura, for all his support during the development of this thesis, for his patience, motivation, enthusiasm and for his enlightening scientific guidance.

Second, I would like to thank to my dear friends and colleagues, Duarte Dias, Filipe Jesus, João Carvalho, João Mendes, Mariana Branco, Miguel Vaz and all other members from “Ventura Group” for their warm friendship and support.

I also would like to thank to all people who participated in the user studies conducted in this thesis, specially to my colleague Henrique Delgado, who also supported me during this thesis. Without their contribution this work would not have been possible.

I would like to thank my family, specially my parents, grandparents and brother, who gave me support and stayed by my side during the most difficult moments. Last, but not least, I would like to specially thank my dear friends, for all the support, motivation and inspiration in the writing of this thesis.

Abstract

Several methods have been proposed in the literature to address the problem of automatic mapping by a robot using range scan data, under localization uncertainty. Most methods rely on the minimization of the matching error among individual depth frames. However, ambiguity in sensor data often leads to erroneous matching (due to local minima), hard to cope with in a purely automatic approach.

This thesis addresses the problem of scan matching by proposing a semi-automatic approach, denoted interactive alignment, involving a human operator in the process of detecting and correcting erroneous matches. Instead of allowing the operator complete freedom in correcting the matching in a frame by frame basis, the proposed method constrains human intervention along the degrees of freedom with most uncertainty. The user is able to translate and rotate individual point clouds, with the help of a force field-like reaction to the movement of each point cloud. The theoretical framework is initially formulated in the 2D space, and then extended to the 3D space, where the user interaction with point clouds becomes non-trivial due to the increase of degrees of freedom.

A graphical user interface was implemented to test both frameworks. Experimental results using LIDAR data are presented to validate empirically the approach, together with a user study to evaluate the benefits of the approach. Experiments using RGB-D data, provided by the Kinect sensor, were also conducted together with a user study that shows the importance of the proposed method in the alignment process, in the 3D space.

Keywords

Scan-matching, Registration adjustment, Mapping, Iterative Closest Points, User interaction, Interactive Interfaces

Resumo

Muitos métodos que tratam do problema do mapeamento automático utilizando sensores de distancia, já foram propostos na literatura. Esses métodos baseiam-se na minimização do erro de correspondências entre *frames*. No entanto devido a ambiguidades que existem nos dados do sensor, o mapa pode conter erros no alinhamento que são difíceis de lidar numa abordagem puramente automática.

Esta tese aborda o problema de alinhamento entre *frames* de uma forma semi automática, propondo um método, denominado "Alinhamento Interactivo", onde os utilizadores detectam e corrigem os erros no alinhamento. Em vez de dar liberdade ao utilizador para corrigir o alinhamento, o método proposto restringe a interactividade ao longo dos graus de liberdade com maior incerteza. O utilizador é capaz de transladar e rodar *scans* com ajuda de um campo de forças de acção-reacção. O formalização matemática do sistema de forças foi inicialmente desenvolvida para o espaço 2D e posteriormente estendida para o espaço 3D, onde a interacção com as nuvens de pontos (*3D frames*) torna-se não-trivial devido ao aumento dos graus de liberdade.

Para testar o método proposto foram implementadas duas interfaces (uma para cada espaço dimensional). As nuvens de pontos usadas nos testes foram obtidas usando um laser *LIDAR* (para 2D) e um *Kinect* (para 3D). Para validar o método proposto, foram realizados estudos com os utilizadores em ambos os espaços dimensionais. Os resultados obtidos pelos utilizadores mostram a utilidade e importância do método na correcção do alinhamento de nuvens de pontos.

Palavras Chave

Correspondência entre nuvens de pontos, Correcção do alinhamento entre nuvens de pontos, Mapeamento, Método iterativo dos pontos mais próximos, Interacção com os utilizadores, Interfaces interactivas

Contents

List of Figures

List of Tables

List of Algorithms

Abbreviations

ANOVA analysis of variance

DoF Degrees of Freedom

EKF Extended Kalman Filter

GUI Graphical User Interface

ICP Iterative Closest Points

IST Instituto Superior Técnico

Kd-trees K-dimensional trees

LIDAR Light Detection And Ranging

MSc Master Science

ORB Oriented FAST and Rotated BRIEF

RANSAC RANdom SAmple Consensus

SaR Search and Rescue

SIFT Scale-Invariant Feature Transform

SLAM Simultaneous Localization and Mapping

SURF Speeded Up Robust Features

List of Symbols

Greek symbols

τ	Total torque
τ_m	Mouse torque
τ_r	Reaction torque
ξ_{pot}	Threshold which defines the Potential
ξ_t	Threshold for balancing forces using translations
ξ_θ	Threshold for balancing forces using rotations in the 2D space
ξ_R	Threshold for balancing forces using rotations in the 3D space
ξ_{CP}	Threshold for closest points
ξ_{CP}^{max}	Maximum threshold for closest points
ξ_T	Threshold for testing the ICP convergence
θ	2D rotation angle
α	Euler angle to rotate around the x axis
β	Euler angle to rotate around the y axis
γ	Euler angle to rotate around the z axis
δ	Angular difference between to sequential rotations
μ	Mean
σ	Standard deviation
η	Surface normal

Roman symbols

M	Model scan
D	Data scan
m_k	Points from Model scan
d_k	Points from Data scan
n	Total number of scans in a graph
N	Number of pairs of closest points
N_M	Total number of points in the Model scan
N_D	Total number of points in the Data scan
R	Rotation matrix
t	Translation vector
T	Generic homogeneous rigid transformation
$T^{[0]}$	Initial estimation of an homogeneous rigid transformation
T_i^{i-1}	Homogeneous rigid transformation between scan i and $i-1$
T_t	Translation homogeneous transformation
T_R	Rotation homogeneous transformation
p_f	Mouse current position
p_o	Mouse initial position (before drag)
c	Point cloud centroid
J_m	Mouse potential function
J_r	Reaction potential function
F_m	Mouse force
F_r	Reaction force
k_m	Mouse force and torque proportionality constant
k_r	Reaction force and torque proportionality constant
k_{CP}	Proportionality constant used in the rejection step of the ICP algorithm
P	Subset of pairs of closest points
u	Rotation axis
j_{max}	Maximum number of iterations for the ICP algorithm
$\tilde{x}$	Median
C^M	Covariance matrix associated with the measured points from point cloud M
C^D	Covariance matrix associated with the measured points from point cloud D
c_x, c_y, f_x, f_y	Camera intrinsic parameters

1 Introduction

Contents

1.1 Motivation

The problem of scan-matching has been an active field of research over the past years. The problem has been studied for 2D and 3D applications, specially the last one, has grown in popularity and found increasing applications in fields including medical imaging [1], object modelling [2], and robotics [3].

Methods to address the problem of scan-matching have been proposed and used in many applications, in particular for 3D mapping of an environment (see [4] for a review). These methods vary both in terms of sensors used (e.g., sonars [5, 6], LIDAR [7, 8], vision [9, 10], and more recently 3D range sensors [11, 12]), and in methodologies (e.g., probabilistic [5, 6], scan-matching [7, 13]).

Accurate 3D models of the environment can be very useful for locating a camera view in a pre-computed map, for measuring dimensions and get lengths and sizes of objects, for free exploration and photorealistic rendering of the environment or can even be used in Search and Rescue (SaR) applications for better mission planning. However, building these maps is not an easy task. Frame-to-frame matching can fail for many reasons. Most of the scan-matching methods are prone to local minima, originated, for instance, by ambiguity in the sensor data or by locally periodic patterns in the environment.

When a user attempts to build a map with an automatic scan-matching method (e.g ICP, see section 2.2) alongside a vision-based mapping algorithm (see section 2.3) using a depth range camera (e.g. Kinect), the matching between frames can specially fail if the user moves the camera too fast (leading to motion blur in the images) or even if he is careful, the field of view of the camera may not contain sufficient color and geometric features to successfully align the frames (Fig. 1.1(a)).

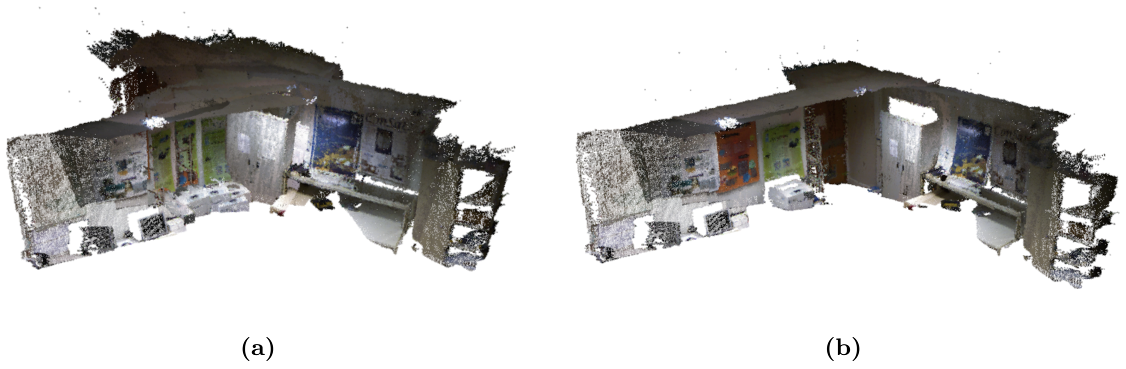

(a) **(b)**

Figure 1.1: (a) Map done using a scan-matching algorithm (see section 2.2) together with a vision-based mapping algorithm (see section 2.3), containing errors in the alignment of some pairs of frames. (b) Map with the alignment between frames corrected using the proposed method presented in this thesis (see chapter 3).

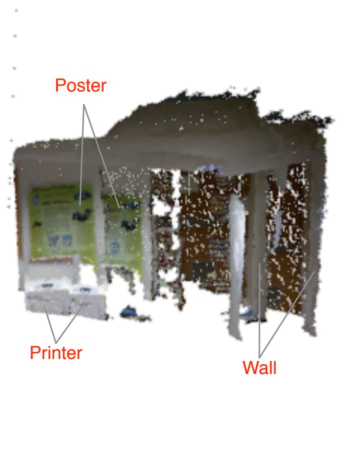

(a)

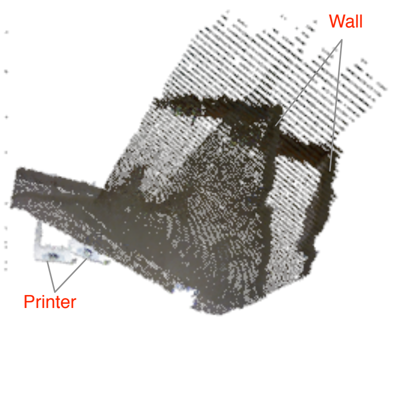

(b)

Figure 1.2: (a) Front view of two misaligned scans. (b) Top view of two misaligned scans.

Moreover, the loop closure problem remains a not completely solved problem [14, 15]. Approaches aiming at global consistency [7, 13] have been proposed, however, they are often computationally complex, and yet prone to error when faced with missing data.

By looking at Fig. 1.2, one can easily see how the two scans fit together. For instance, it is possible to identify a printer, a wall and a poster. Based on the empiric experience, we believe that users have the perception to identify certain patterns in both images, allowing them to be capable of interfering with the scan-matching, in order to correct it (Fig. 1.1(b)). The quantification of this perception and ability is not the subject of this work, but it is built over this assumption.

1.2 Objectives

The main objectives of this thesis are to:

1. Develop an interactive system where users interact with pairs of scans (2D and 3D scans), in order to correct the wrong alignment obtained by automatic scan-matching methods.
2. Develop a method to help the users in the alignment process;
3. Obtain accurate indoor maps by using the proposed approach, together with an automatic method.

1.3 Literature Review

This section presents and discusses some work already done in the area of interactive mapping and human-interface interaction.

1.3.1 Interactive Mapping

The work that have already been done in the field of interaction between users and scan ranges focus on interactive systems which enable users to help in the mapping process of indoor spaces.

Dellaert and Bruemmer in [16], instead of using the traditional Simultaneous Localization and Mapping (SLAM) to map the environment, they proposed the Semantic SLAM which introduces a "collaborative cognitive workspace" for dynamic information exchange between robots and users to collaboratively construct the map. In their system, users use an interactive visual display to add, verify, remove, or annotate abstractions within the map. For instance by clicking on certain entities and query the "state of mind" of the robot, it presents an alternative interpretation of the environment and their relative probabilities (e.g. "there is a 70% probability of this object be a temporary obstacle and a 30% chance of being part of the map"). The robot can also use the map to communicate with the user graphically, for instance, by highlighting areas that have already been searched.

Diosi et al. in [17], presented an interactive framework that enables a robot to generate a segmented metric map of an environment by following a user and storing virtual location markers created through verbal commands. In their system, an occupancy grid map is generated, with segmented information describing the extent of each region of interest. To build the map, the robot uses SLAM while following autonomously a tour guide, who describes each location in the tour using simple voice commands (e.g. "Robot, we are in the Lab"). After generating the map, the robot can be sent back to any location using a voice command (e.g. "Robot, go to the lab").

Recently, 3D range sensors, such as the Kinect sensor from Microsoft, have been emerging in the community and are being used in many fields of research such as 3D objects modelling and 3D mapping. This sensors sensors are equipped with a RGB and a Depth camera, capable of providing dense color and depth information. However, their field of view is limited (about 60^o), the data is very noisy and have low resolution (640x480). Even so, some interesting work in the field of interactive 3D mapping was done using such sensors [10, 18].

Sinha et al. in [10], presented an interactive system for generating photorealistic, textured, piecewise-planar 3D models of architectural structures and urban scenes from unordered sets of photographs. To obtain 3D model of the environment, they use algorithms to detect features in all images, which are then matched across image pairs, and used to estimate the camera poses and positions of points in the 3D space. Afterwards, lines are extracted and used to automatically estimate vanishing points in the scene. The extracted 2D lines in each image are assigned vanishing directions that are consistent across the entire collection. Users then seat in front a computer and use an interactive 3D interface to sketch 2D outlines of planar sections of the scene by drawing over photographs. Their system allows the users to visualize, edit and refine the geometry of the scene. As the 3D geometry is created the photographs are projected onto its surfaces, providing visual feedback during geometric editing. With this work, one is able to correct structures in the model, in order to get a proper 3D model of the environment. However, the proposed system works after having a rough 3D model of the environment, which is obtained, in this case, by feature matching. If the feature matching for some reason fails, point clouds will not be aligned. The proposed system does not permit correct the wrong alignment between frames. This thesis focus precisely on solving this alignment problem using also an interactive approach.

Another work on interactive 3D modelling was presented by Du et al. in [18]. They built a prototype system that runs in real-time on a laptop, assisting and interacting with a user on-the-fly. Their system is capable of scanning large-scale indoor spaces. To built the 3D maps, they sequentially get frames from a Kinect sensor, and do frame-to-frame registration by matching the current frame with the most recent frame. To align each pair of frames, they get visual features from RGB images and then use them in the algorithm described in [19]. While the map is being built, and in order to achieve robustness and completeness in the 3D mapping, users are able to intervene with the mapping in three situation:

1. When for some reason the system fails in detecting visual features (e.g. the user moved the camera to fast), the system stops mapping, and ask the user to move the camera to a previous seen scene. The user can either "undo" and drop the most recent frames (e.g. remove frames of an intruding person) or "rewind" to any previous frame in the system and "resume" at a different point.

2. When mapping, missing areas exist in the scene either because those areas have never been captured or the frames from the map did not get depth values (e.g. because of camera range or surface slant). The system is capable of estimating the completeness of the map, and with this, it is able to suggest places where the user should go, in order to get missing data in the map.

3. Automatic loop closure is hard to perform, so the system runs an automatic matching algorithm to select candidates frame pairs, and by using a visibility criterion, the system suggests frames pairs with large visibility conflicts. Users can then select any frame pair to perform their alignment using an automatic algorithm (such as the one in [20] and [21]), and add loop closure constrains. They can also inspect the resulting map and decide either accept or reject the newly added constrain.

With this work the authors showed very promising results with large indoor maps, and implemented an interesting interactive system where users help with the mapping process. However the system highly depends on the feature matching between scans. There are some cases where algorithms are unable to detect features. For instance, if the map had a room with white walls, the proposed system would not have permitted the user to enter into room. Even if the feature matching fails and the alignment between frames comes wrong, the system does not offer ways to correct it. To solve this problem, the method proposed in this thesis also uses the help of the users but to manually correct the misalignment.

1.3.2 Human-Interface interaction

Many applications require interaction between a user and a computer interface using a computer mouse. For instance, in the field of computer graphics users often interact and manipulate visual images or 3D objects. The interaction with objects is usually performed by applying translations and rotation to them (e.g. Meshlab[1]). In the 2D space this kind of interaction is rather trivial to perform,

[1]Meshlab is an open source, portable, and extensible system for the processing and editing of unstructured 3D meshes (http://www.meshlab.sourceforge.net, online on 10-Oct-2012)

however it becomes harder when 2D controllers are used to manipulate objects in the 3D space, due the increase of the Degrees of Freedom (DoF).

Applying rotations to 3D objects using 2D controllers is not an easy task. Chen et al. in [22] described and evaluated the design of four virtual controllers to rotate objects using a computer mouse. They conducted a user study, where users were asked to manipulate 3D objects using four types of controllers: two of them with graphical sliders to control each degree of freedom, one to control the three DoF by moving the mouse up-down, left-right and in the diagonal, and one that simulates the mechanics of a physical 3D trackball that can freely rotate about any arbitrary axis in the 3D space (virtual sphere). The study showed that the users preferred the last controller (virtual sphere) over the others for being more "natural".

Later, Bade et al. in [23] did an usability comparison of four mouse-based interaction techniques based on four principles for 3D rotations techniques. Two of the techniques used in the study were an improvement to the virtual sphere proposed by Chen et al. in [22] (the Bell's Virtual Trackball and the Shoemake's Virtual Trackball), the third one was the Two-Axis Valuator Trackball also described in [22] and the last one was a variant of the previous one. The comparison was evaluated with a user study, which aimed to see which rotation method was most comfortable and predictable for the users. The study showed that users preferred the "Two-Axis Valuator Trackball".

Recently Zhao et al. in [24] also did a comparison between the same rotation methods as Bade et al., but in all techniques the third degree of freedom was controlled by the mouse-wheel. In the user study they did, they did not find significant performance difference for each method. Although most users gave positive feedback on using the mouse wheel, it is important to note that the increment of the wheel must be carefully adjusted overtime because there are times when users want to perform large rotations and other times when users just want to do slight rotations.

1.4 Approach

To carry out the main objective, an alternative approach to the scan-matching is proposed. A human-in-the-loop of the scan matching process is considered. In particular, the user is invited to interact with the matching process, by adjusting the match of individual pairs of scans. This adjustment is however constrained by favouring adjustments along the directions of greater ambiguity. Take for instance a case of pairs of identical scans taken from an homogeneous corridor (schematized in Fig. 1.3, a pair of 2D scans are used here for simplicity sake). The system should favour the adjustment of the scans along the corridor, while disfavouring movements orthogonal to the corridor.

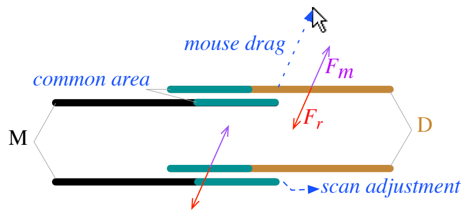

Figure 1.3: Top view of 2 corridors. The scan D is adjusted such that the reaction force F_r, computed from the cost function gradient, balances the force F_m imposed by the mouse drag. Scan M and D are correctly aligned when both common areas are overlapping.

The proposed method is based on a Graphical User Interface (GUI), where the user interacts with the system using a common computer interface (mouse and keyboard). Consider a pair of range scans denoted M (for model) and D (for data). Fig. 1.3 illustrates the situation for the corridor example. When the user drags one of the range scans, say scan D, using the mouse, a corresponding virtual force F_m is produced (proportional to the drag vector). Opposing it, a reaction force F_r is computed based in the match between scans M and D. Considering the scan-matching cost function as a potential function, the symmetric of its gradient with respect to the shift of scan D can be seen as a reaction force F_r. This reaction force "attracts" scan D towards M, along the direction of less ambiguity. Scan D is then moved such that both forces become balanced, $F_m + F_r = 0$. In the corridor example of Fig. 1.3, the reaction force is dominantly orthogonal to the corridor axis.

The proposed method was first developed and tested in the 2D space and then extended to the 3D space. A Nomadic Scout robot with a Light Detection And Ranging (LIDAR) onboard is used to take 2D scans while a Microsoft Kinect sensor is used to obtain 3D scans. In both dimensional spaces, scans are sequentially obtained and the current frame is matched with the most recent frame by computing a rigid transformation. Both scans and transformations are organized in a data structure kept in the computer memory, and can be used for posterior analysis at any time.

To build the map of the environment, the Iterative Closest Points (ICP) algorithm (see section 2.2) is used to obtain the initial rigid transformation between M and D automatically. Then, the proposed method is used to correct any ambiguity in the alignment. Note that there are other automatic scan-matching algorithms[2] that have better performance than ICP. The ICP is used for the sake of simplicity.

1.5 Main Contributions

This thesis addresses the problem of scan-matching using an interactive approach. In order to align pairs of scans or point clouds, users interact with them through a GUI using a simple computer mouse and keyboard. To help the users in the alignment process, this thesis contributed with a method, called "Interactive Alignment", which uses virtual forces to restrain the movement of the range scans. Scans are aligned by balancing a force produced by a mouse drag (mouse force) with a reaction force produced by a potential field (reaction force). The proposed method was first developed in the 2D

[2]see RGBDSLAM in http://www.ros.org/wiki/rgbdslam (retrieved 10-Oct-2012)

space and the extended to the 3D space, and does not require an initial alignment between frames to work. To validate the method, an user study is presented for each dimensional space (2D and 3D).

The following publications resulted directly from this thesis:

1. 10th IEEE International Symposium on Safety Security and Rescue Robotics (SSRR 2012), [25]
2. 17th IEEE International Conference on Emerging Technologies & Factory Automation (ETFA 2012), [26]
3. 1st International Workshop on Perception for Mobile Robots Autonomy (PEMRA 2012), [27]
4. Journal of Automation, Mobile Robotics & Intelligent Systems (JAMRIS), [28] (in press)

1.6 Thesis Outline

This dissertation is organized as follows: Chapter 2 provides background on the shape-based registration problem and presents the registration method used in this dissertation. Ways of handling outliers in the Data, and for dealing with convergence to local minima are discussed. Also, the method represent range scans in memory, as well as how the map is build from them is described. Chapter 3 proposes the method for interactive mapping. First, the method is formalized for the 2D space and then expanded to the 3D space. Chapter 4 presents the results together with an user study conducted to evaluate the performance of the proposed method in each dimensional space (2D and 3D). Finally, Chapter 5 draws some conclusions and discuss possible future work directions. Appendix A and B covers details concerning the interactive interfaces implemented in this thesis, and appendix C has the results obtained in both user studies.

2 Registration Problem

Contents

The goals of this chapter are to provide background on the shape-based registration problem, familiarize the reader with the registration solution method used in this dissertation, and present the data structure used to keep map in the computer memory.

2.1 Problem Statement

Registration is the problem of determining the relative pose (position and orientation) between two scans of the same scene (or object). This is done by using features from both scans. Features can be either geometric or photometric, and 2D or 3D. The main goal of registration is to find a spatial transformation which brings the features from both scans into alignment as measured by a suitable cost metric. The transformation may be either rigid or deformable, and may or may not include a scale term. The work presented in this thesis concentrates on the problem of rigid registration without scale of 2D and 3D geometric features. Figure 2.1 shows the basic steps to do the registration of two scans.

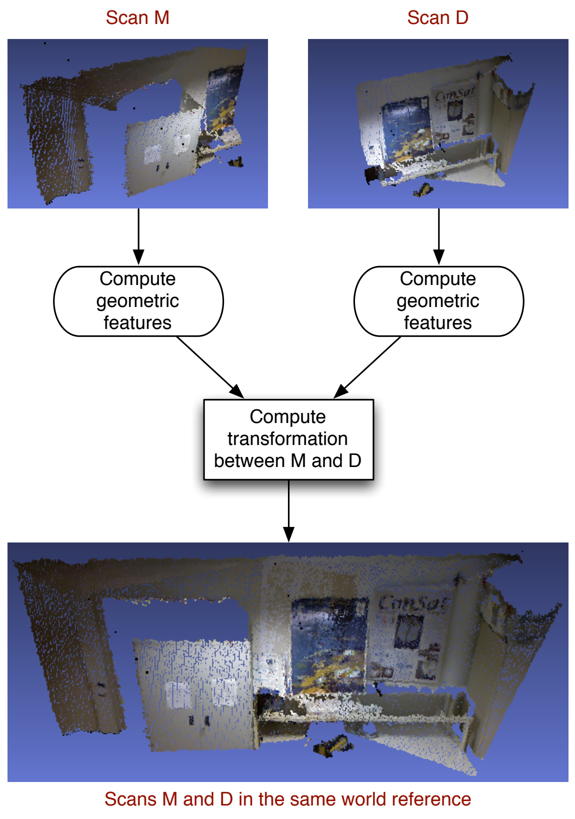
Scan M
Scan D
Compute geometric features
Compute geometric features
Compute transformation between M and D
Scans M and D in the same world reference

Figure 2.1: Registration problem overview

2.2 Iterative Closest Points Algorithm

For the more general class of registration problems, pairs of correspondences, $[m_k, d_k]$, are unknown a priori. In order to solve this problem, Besl and McKay proposed in [21] the ICP algorithm. Given two range scans, M and D, and an initial estimation $T^{[0]}$, the ICP algorithm computes the best rigid transformation, T, that better aligns, D with M. The approach of the algorithm consists in minimizing the distance between pairs of correspondences from the two scans iteratively. A diagram explaining conceptually the algorithm is presented in Fig. 2.2.

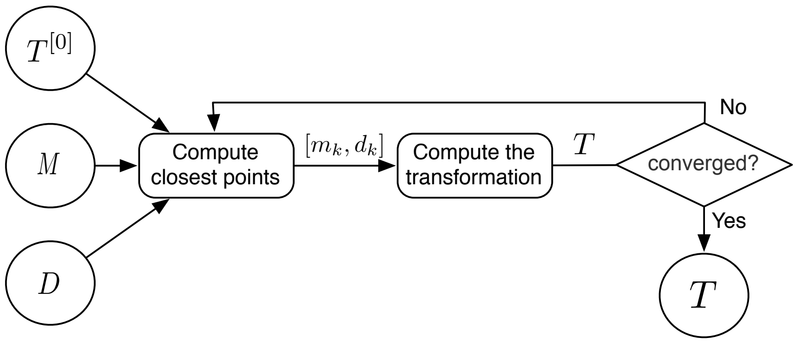

Figure 2.2: Diagram of the ICP Algorithm

The ICP algorithm works as follows:

1. Initialize the cumulative homogeneous transformation T with the identity transformation. Reset the iteration counter, j, to zero.

2. For each discrete point d_k in scan D, compute the closest point (in terms of Euclidean distance) m_k which lies on the surface of scan M.

3. Using the correspondences pairs obtained from the previous step, find the transformation T_k which minimize the distance between them.

4. Apply the incremental transformation from step 3 to all points of scan D, d_k. Update the cumulative transformation, T, based upon the incremental transformation T_k:

$$T \leftarrow T_k \, T \tag{2.1}$$

5. If the stopping criterion is satisfied, terminate and return T, else go back to step 2.

There are several stopping criteria which can be used with ICP. In this dissertation the following two stop criteria are used:

- Stop if the incremental transformation absolute magnitude is less than a threshold:

$$|T_k| < \xi_T \tag{2.2}$$

- Stop if the total number of iterations exceeds a threshold: $j > j_{max}$. This condition takes effect if the previous one is not triggered.

To better understand how the algorithm works, Fig. 2.3 shows an example of two scans from a corridor being aligned. In the example both scans have a part in common, and a part that only belongs to each scan. For the sake of simplicity the example is given in the 2D space and the algorithm is supposed to converge in two iterations.

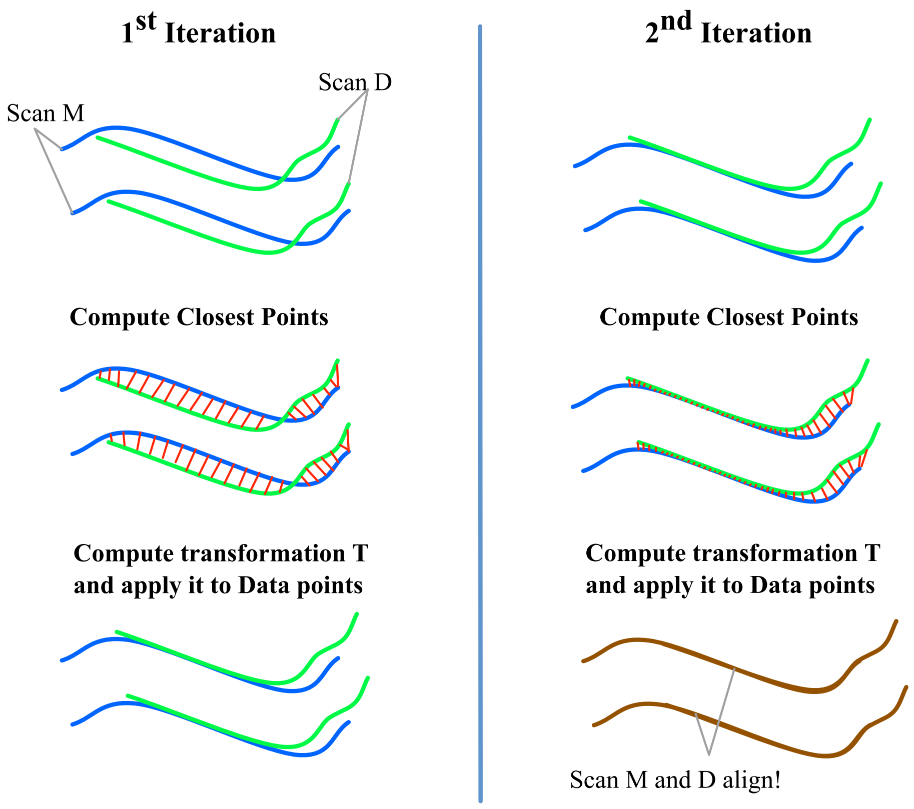

1st Iteration
2nd Iteration
Scan D
Scan M
Compute Closest Points
Compute Closest Points
Compute transformation T and apply it to Data points
Compute transformation T and apply it to Data points
Scan M and D align!

Figure 2.3: Example of two portions of a corridor (Scan M and D) being align with the ICP algorithm. In blue is the scan M, in green is the scan D and the red strokes are the distance between closest point from both scans.

2.2.1 Closest Points

In each iteration, the ICP algorithm starts by computing pairs of points composed by matched points from each scan, which are then used to find the transformation that align both scans. These pairs of points are created by computing the closest points from one scan (D) to the other (M). The diagram presented in Fig. 2.4 shows the steps done by the algorithm to get these pairs of points.

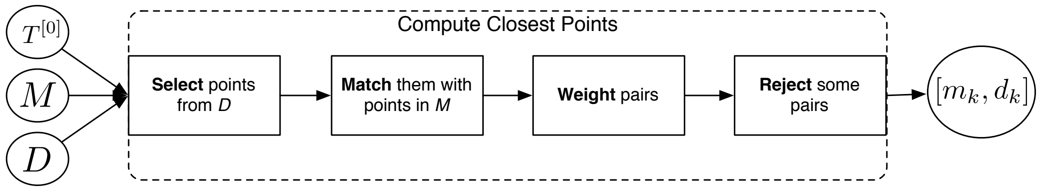

Figure 2.4: Diagram showing the steps to compute the closest points to each scan.

Each stage of the algorithm can be implemented using methods that have already been proposed in the literature. In particular, Rusinkiewicz and Levoy did a comparison between methods for each stage of the algorithm in [29] with respect to time (number of iterations needed by ICP to converge) and performance, and proposed a high-speed ICP algorithm variant.

For the **Selecting** stage of the algorithm, one can use all points available in the scan, like Besl did when introduced the ICP algorithm in [21] or simply random sampling with a different sample of points at each iteration, like Masuda did in [30]. The ICP implemented in this thesis, uses all points when the data obtained from the sensor is below a threshold (number of point below 1000), otherwise uses random sampling as suggested by Rusinkiewicz and Levoy in [29]. In the end of this stage a set of points from scans D is obtained: $\{d_k\}$.

The most computationally expensive step in the ICP algorithm is finding the closest points. Although Rusinkiewicz and Levoy suggested using projection-based algorithm to generate point correspondences in the **Matching** stage, in this thesis K-dimensional trees (Kd-trees) are used to compute closest points. Kd-trees are special cases of binary space partitioning trees used to organizing points in a k-dimensional space. Zhang demonstrated in [31] that the average complexity of a closest point query can be reduced from $O(N_D\,N_M)$ to $O(N_D log N_M)$ using these trees (where N_M and N_D are the number of points in scans M and D respectively). By building the tree of scan M and searching in it for the closest point to $\{d_k\}$, pairs of correspondences $[m_k, d_k]$ are obtained.

After obtaining the points correspondences, pairs are weighted in the **Weighting** stage of the algorithm, based on the distance between points in each pair. As suggested by Rusinkiewicz and Levoy, in this thesis, constant weighting is also used to weight pairs. The method is shown in algorithm 2.1 where w_k is the weight of pair k and ξ_{CP}^{max} is the maximum distance allowed between points in one pair.

Finally, in the last stage of the algorithm, the **Rejecting**, pairs that have weight equal to zero are discarded. In end of this stage a new set of pairs $[m_k, d_k]$ is obtained, and is ready to be used in the last step of the ICP algorithm. In each iteration of the algorithm, scans M and D get near to each other. If the same threshold ξ_{CP}^{max} is used in each iteration, some outliers pairs might not be rejected.

Algorithm 2.1 Weighting

```
if $||m_k - Td_k|| < \xi_{CP}^{max}$ then
    $w_k \leftarrow 0$
else
    $w_k \leftarrow 1$
end if
```

In order to improve the outliers removal, Zhang proposed in [31] a method to adaptively update ξ_{CP}^{max} in each iteration by analysing distances statistics (algorithm 2.2).

Algorithm 2.2 Threshold update for better outliers removal

```
if $\mu < \xi_{CP}$ then                          ▷ The registration is quite good
    $\xi_{CP}^{max} \leftarrow \mu + 3\sigma$
else if $\mu < 3\,\xi_{CP}$ then                   ▷ The registration is still good
    $\xi_{CP}^{max} \leftarrow \mu + 2\sigma$
else if $\mu < 6\,\xi_{CP}$ then                   ▷ The registration is not too bad
    $\xi_{CP}^{max} \leftarrow \mu + \sigma$
else                                               ▷ The registration is really bad
    $\xi_{CP}^{max} \leftarrow \tilde{x}$
end if
```

The update of threshold ξ_{CP}^{max} is based on the mean μ and the sample deviation σ of the distances between points in each pair:

$$\mu = \frac{1}{N}\sum_{k=1}^{N}(m_k - Td_k)\,, \tag{2.3}$$

$$\sigma = \sqrt{\frac{1}{N}\sum_{k=1}^{N}((m_k - Td_k) - \mu)^2}, \tag{2.4}$$

where $(m_k - Td_k)$ is the distance between points in pair k and N is the number of pairs. If the registration is really bad, ξ_{CP}^{max} is updated with the median of the distances ($\tilde{x}$). Note that before the ICP algorithm starts, the threshold ξ_{CP}^{max} is set to $k_{CP}\,\xi_{CP}$, where k_{CP} is a proportional constant and ξ_{CP} is a threshold used to check the quality of the registration. The method used to choose the the value of the proportionality constant and the threshold can be found in [31].

2.2.2 Transformation Computation

The last step of the ICP algorithm consists in assigning an error metric based on the pairs of points, previously obtained, and minimizing it. The following three error metrics have been studied:

1. Point-to-Point;
2. Point-to-Plane;
3. Plane-to-Plane.

The **Point-to-Point** error metric consists in computing the best rigid transformation by minimizing the sum of squared distances between corresponding points:

$$T = \arg\min_{T}\sum_{k=1}^{N}\|m_k - T\,d_k\|^2, \tag{2.5}$$

where N is the number of pairs, $\{m_k\}$ and $\{d_k\}$ are respectively points from M and D in homogeneous coordinates and T is the rigid transformation in homogeneous coordinates:

$$T = \left[\begin{array}{c|c} R & t \\ \hline 0 & 1 \end{array}\right], \tag{2.6}$$

with

$$\det(R) = 1 \text{ and } R^T R = I. \tag{2.7}$$

This error metric has closed form solution for determining the rigid transformation that minimizes the error. Some solution methods have been proposed: Arun et al. in [32] proposed a solution based on singular value decomposition, Horn et al. proposed a solution based on quaternions and orthonormal matrices in [33] and [34] respectively, and Walker et al. proposed a solution based on dual quaternions in [35]. Eggert et. al. in [36] evaluated the numerical accuracy and stability of each of theses methods, and concluded that the differences among them were small.

The **Point-to-Plane** error metric was originally introduced by Chen and Medioni [37] as a more robust and accurate variant of standard ICP. This error metric consists on minimizing the sum of squared distances from each source point (m_k) to the plane containing the destination point (d_k) and the oriented perpendicular normal. The new cost function differs from (2.5) by taking into account the surface normals at the source point:

$$T = \arg\min_T \sum_{k=1}^{N} \|\eta_k \cdot (m_k - T\,d_k)\|^2, \tag{2.8}$$

where η_k is the surface normal at m_k. The Point-to-Plane error metric does not has any closed-form solutions available. However the least-squares equations may be solved using a generic non-linear method (e.g. Levenberg-Marquardt), or by linearising the problem as Kok-Lim Low did in [38] by assuming that incremental rotations are small: $\sin(\theta) \sim \theta$ and $\cos(\theta) \sim 1$.

The **Plane-to-Plane** error metric, also known as generalized ICP, was introduced by Segal et al. in [39] as an improvement to the Point-to-Plane error metric. They proposed to merge the Point-to-Point and Point-to-Plane error metrics into a single probabilistic framework, and devised a generalised framework that naturally converges to both of them by appropriately defining the sample covariance matrices associated with each point. The way that the generalized ICP cost function is derived is described in [39] and have the following form:

$$T = \arg\min_T \sum_{k=1}^{N} (m_k - Td_k)^T \left(C_k^M + TC_k^D T^T\right)^{-1} (m_k - Td_k), \tag{2.9}$$

where C_k^M and C_k^D are covariance matrices associated with the measured points from scan M and D respectively.

The Point-to-Point error metric can be obtained by setting $C_k^M = I$ and $C_k^D = 0$:

$$\begin{aligned} T &= \arg\min_T \sum_{k=1}^{N} (m_k - Td_k)^T (m_k - Td_k) \\ &= \arg\min_T \sum_{k=1}^{N} \|(m_k - Td_k)\|^2, \end{aligned} \tag{2.10}$$

which is identical to (2.5). This also shows that Point-to-Point error metric does not takes into account the structural shape of each scan.

The Point-to-Plane error metric is obtained by setting $C_k^M = P_k^{-1}$ and $C_k^D = 0$, where $P_k = \eta_k^T \eta_k$ is the projection onto the span of surface normal at m_k:

$$\begin{aligned} T &= \arg\min_T \sum_{k=1}^{N} (m_k - Td_k)^T P_k (m_k - Td_k) \\ &= \arg\min_T \sum_{k=1}^{N} \|\eta_k \cdot (m_k - Td_k)\|^2. \end{aligned} \tag{2.11}$$

This cost function is identical to (2.8). This also shows that Point-to-Plane error metric only takes into account the structural shape of scan M.

The Plane-to-plane is obtained when setting $C_k^M \neq 0$ and $C_k^D \neq 0$. This method improves the ICP algorithm by exploiting the locally planar structure of both scans. This error metric also does not has close form solution. However the problem may be solved using a generic non-linear method (e.g. Levenberg-Marquardt).

2.3 ICP Inicialization

As said before the ICP algorithm receives as input the initial transformation between the two scans being aligned. This transformation can be either initialized with the identity matrix or with a precomputed matrix, and it highly influences the effectiveness of the algorithm.

There are many solutions available in the literature to get the initial transformation between two scans. In this thesis two different methods are used for both 2D and 3D spaces, and using different sensors.

In 2D space, we only have access to the depth information provided by the laser sensor, thus the odometry of the robot together with a simple implementation of an Extended Kalman Filter (EKF) are used get the position and orientation of the sensor along time. Figure 2.5 shows the robot odometry geometry. The transformation which transforms the scans taken at instant n to the coordinates of robot at instant $n-1$, can be obtained by doing:

$$T_n^{n-1} = \begin{bmatrix} \cos(\theta_n - \theta n - 1) & -\sin(\theta_n - \theta n - 1) & x_n - x_{n-1} \\ \sin(\theta_n - \theta n - 1) & \cos(\theta_n - \theta n - 1) & y_n - y_{n-1} \\ 0 & 0 & 1 \end{bmatrix}, \tag{2.12}$$

where $[x_{n-1}, y_{n-1}, \theta_{n-1}]$ and $[x_n, y_n, \theta_n]$ are the positions and orientations of the robot at instant $n-1$ and n respectively. This transformation is then used to initialize the ICP algorithm ($T^{[0]}$).

In the 3D space a Microsoft Kinect sensor was used to get 3D scans. When using a robot with a Kinect onboard, the same method used in the 2D method to obtain the initial transformation can be applied. On the contrary, when the Kinect is used freely by a user, a similar algorithm based on vision features to the one proposed by Henry et al. in [19], can be used. In Fig. 2.6 is presented an overview of the algorithm, which consists in using the information provided by the RGB and depth cameras to compute features from both frames and use them to compute the best rigid transformation that align them.

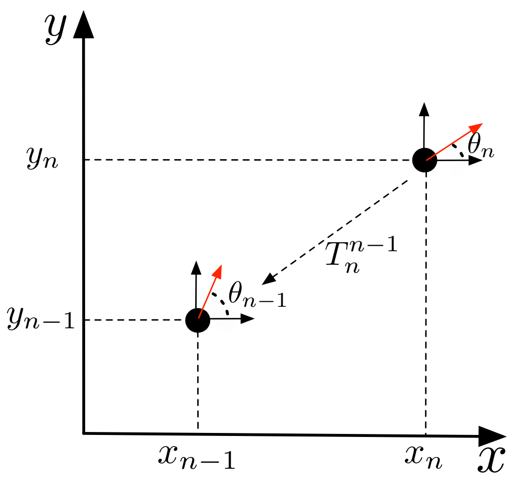

Figure 2.5: Robot odometry geometry. Black dots represent the robot. Red arrows are the orientation of the robot (θ_{n-1} and θ_n). [x_{n-1}, y_{n-1}] and [x_n,y_n] are the robot positions at instant $n-1$ and n respectively. T_n^{n-1} is the transformation that transforms the scans taken at instant n to the coordinates of robot at instant $n-1$.

Algorithm 2.3 Hamming distance

```
function HammingDistance($descriptorA$, $descriptorB$)
    $dist \leftarrow 0$
    for $i = 0$ to 32 do
        if $descriptorA[i] \neq descriptorB[i]$ then
            $dist \leftarrow dist + 1$
        end if
    end for
    return $dist$
end function
```

The first step of the algorithm consists in extracting features from the RGB image of each frame. Some features detectors, like Scale-Invariant Feature Transform (SIFT) and Speeded Up Robust Features (SURF), have already been proposed in [40] and [41] respectively, and used in many applications in computer vision. More recently Ethan et al. proposed the Oriented FAST and Rotated BRIEF (ORB) feature detector in [42] as an improvement to the SIFT and SURF detectors. Although less reliable than SURF and no scale invariant, ORB still behaves with great accuracy for small scale changes and is faster than the other features detectors. Because of this characteristics it was chosen to be used in the implementation.

In the second step of the algorithm the obtained features from each RGB frame are matched together by their similarity. The ORB implementation from Willow Garage[1] returns each descriptor as a set of binary values (32 bytes). A good way to match them is by minimizing the Hamming distance between descriptors. Algorithm 2.3 shows the steps performed to compute this distance and algorithm 2.4 describes the matching process.

The third step of the algorithm uses the information from both depth frames and the intrinsic

[1]Implementation is available on the OpenCV library

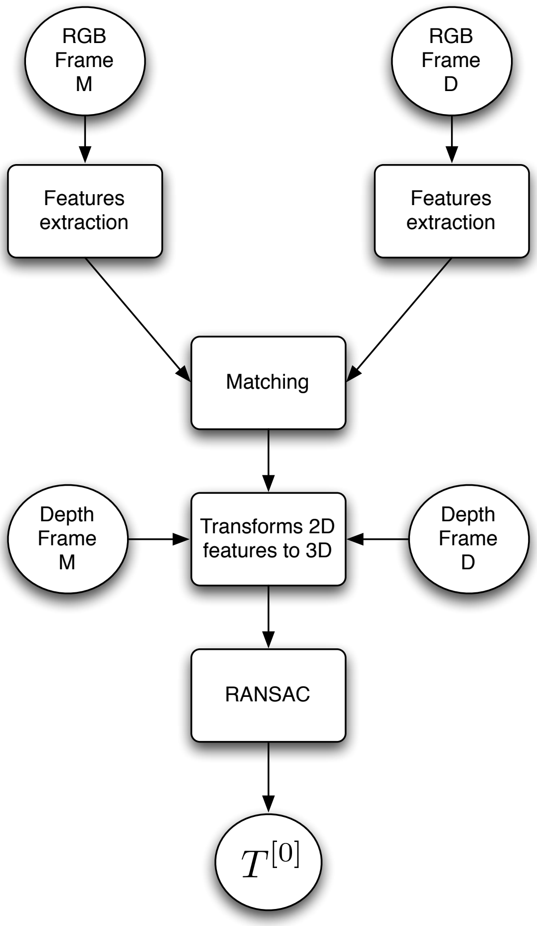

Figure 2.6: Diagram of the Algorithm used to get the initial transformation between frames using a Depth camera with a feature detector.

Algorithm 2.4 ORB Matching process

```
for each $feature$ from Frame 1 do
    $d_1 \leftarrow +\infty$, $d_2 \leftarrow +\infty$
    for each $feature$ from Frame 2 do
        $dist \leftarrow HammingDistance(frame1\_feature.descriptor, frame2\_feature.descriptor)$
        if $d_1 > dist$ then
            $d_2 \leftarrow d_1$
            $d_1 \leftarrow dist$
            $best\_candidate \leftarrow feature$
        else if $d_2 > dist$ then
            $d_2 \leftarrow dist$
        end if
    end for
    if $d_1 < q * d_2$ then
        $feature$ from Frame 1 has a match with $best\_candidate$
    end if
end for
```

parameters of the depth camera to transform the pairs of matched features into 3D pairs of features:

$$\begin{aligned} x &= \frac{u - c_x}{f_x} Z, \\ y &= \frac{v - c_y}{f_y} Z, \\ z &= Z, \end{aligned} \tag{2.13}$$

where (u,v) is the coordinates of a feature pixel, (x,y,z) is the coordinates of a 3D feature, Z is the depth value provided by the depth frame and (c_x,c_y,f_x,f_y) are the depth camera intrinsic parameters. Note that if a feature have $Z = 0$ or $Z = \text{NaN}$ (Not a Number) the corresponding pair is discarded.

Finally, the RANdom SAmple Consensus (RANSAC) method (see [20]) is used in the 3D pairs of features obtained, to estimate the best rigid transformation that align scan M with scan D. RANSAC is an iterative method that estimate parameters of a mathematical model from a set of observed data which contains outliers. In this case the rigid transformation model is used:

$$m_k = T^{[0]}\, d_k, \tag{2.14}$$

where $[m_k,d_k]$ is a pair of 3D features and $T^{[0]}$ is homogeneous rigid transformation constituted by a rotation R and a translation t, which are estimated by RANSAC:

$$T^{[0]} = \left[\begin{array}{c|c} R & t \\ \hline 0 & 1 \end{array}\right]. \tag{2.15}$$

Note that when using a robot, it is possible to use both methods (vision and odometry) to get initial transformation between two consecutive scans, for instance, when the robot enters in a place with low level of features and the vision based method fails, the odometry can be used instead.

2.4 Map Representation

Range scans are obtained sequentially from a range sensor and kept in the computer memory. In this thesis, 2D range scans are obtained with a Nomadic Scout robot with a Hokuyo LIDAR onboard, while 3D range scans are obtained using the Microsoft kinect sensor.

The map is represented by a graph, where each node corresponds to one scan, and each edge connects two scans. Each edge represents the transformation T_i^{i-1} between two consecutive scans, denoted S_{i-1} and S_i. For instance, T_2^1 is the transformation which transforms the coordinate system of scan S_2 into the coordinate system of scan S_1. A representation of the graph is shown in Fig. 2.7.

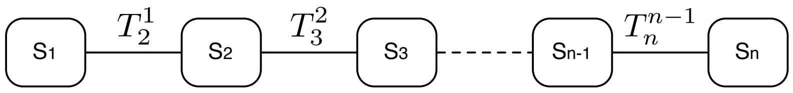

Figure 2.7: Graph representing the map. S_1 to S_n are the scans, T_i^{i-1} is the transformation from scan i to $i-1$, for $i = 2, \ldots, n$, and n is the total number of scans in the graph..

Each scan, S_i, is represented in the sensor coordinate system, so to build the map each scan must be transformed to the world coordinate system. This can be done using the following expression:

$$S_i' = (\prod_{j=1}^{i} T_j^{j-1})\, S_i\,, \quad T_1^0 = I. \tag{2.16}$$

Figure 2.8 and 2.9 show an example of six consecutive scans taken with a Hokuyo LIDAR and a Microsoft Kinect sensor respectively, and the respective map obtained using (2.16).

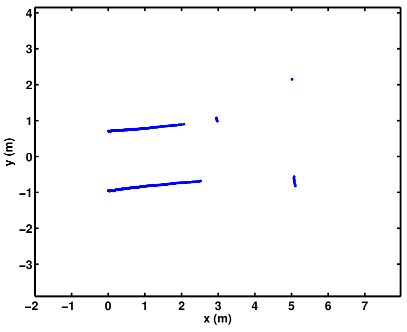

(a) Scan stored in node 1

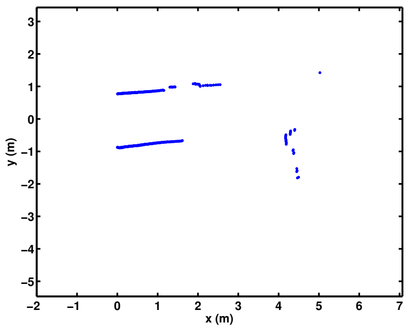

(b) Scan stored in node 2

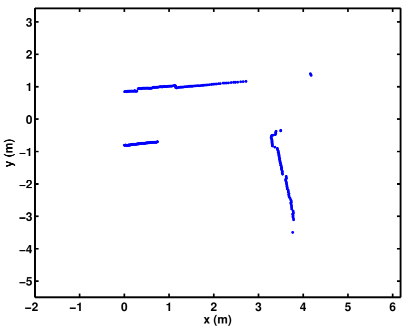

(c) Scan stored in node 3

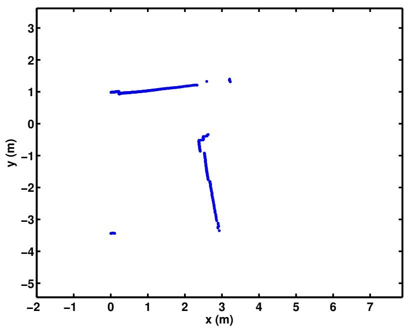

(d) Scan stored in node 4

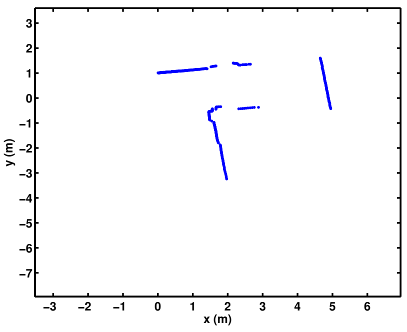

(e) Scan stored in node 5

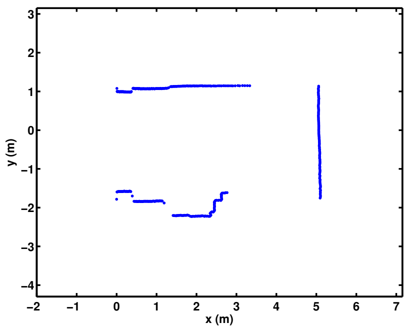

(f) Scan stored in node 6

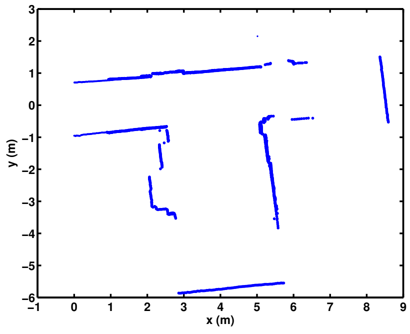

(g) 2D Map

Figure 2.8: (a)-(f) Set of 2D range scans stored in the graph. (g) 2D map built from the scans.

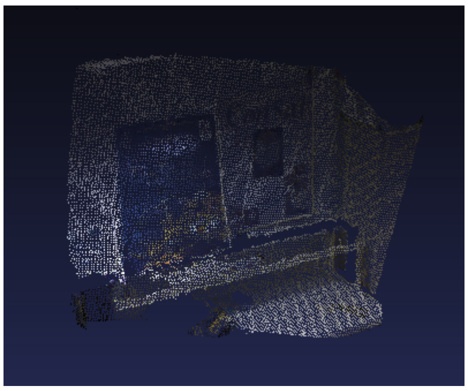

(a) Scan stored in node 1

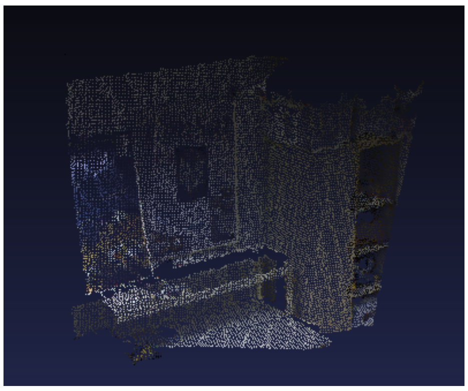

(b) Scan stored in node 2

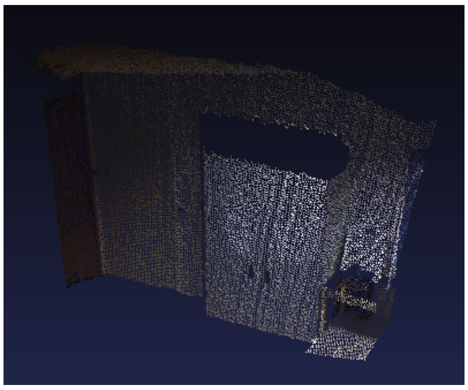

(c) Scan stored in node 3

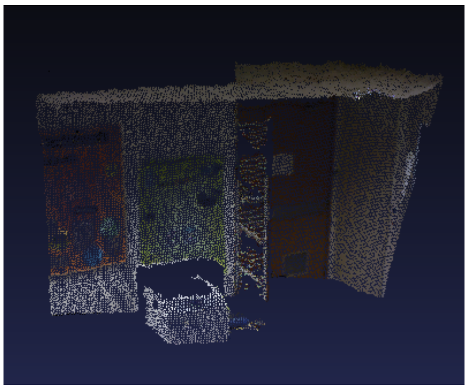

(d) Scan stored in node 4

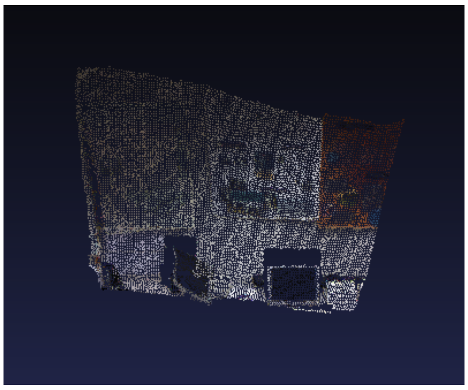

(e) Scan stored in node 5

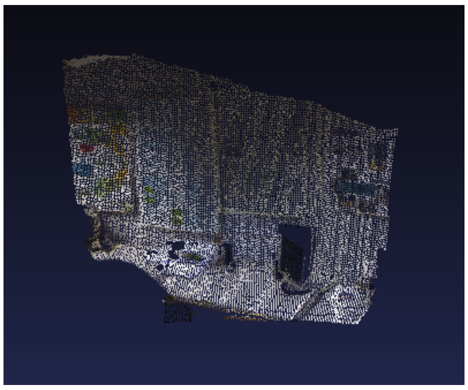

(f) Scan stored in node 6

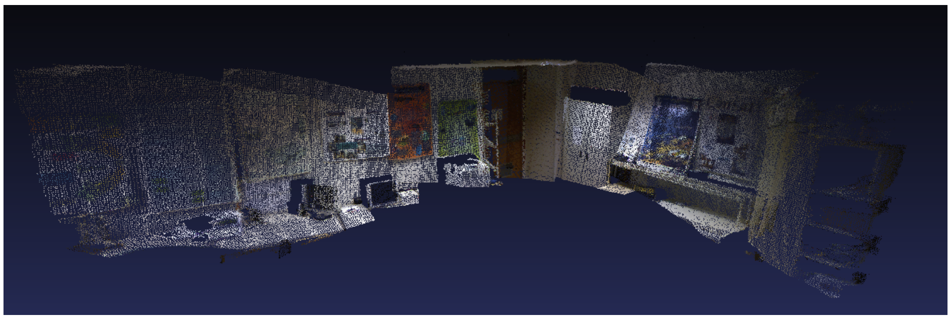

(g) 3D Map

Figure 2.9: (a)-(f) Set of 3D range scans stored in the graph. (g) 3D map built from the scans.

3 Interactive Alignment

Contents

This chapter proposes a semi-automatic method, denoted interactive alignment, which allows and helps the user to interfere with the scan alignment process, in order to correct alignment errors between range scans. The proposed method is based on a force system that restrains the movement of the range scans. The method is initially developed in the 2D space and then extended to the 3D space. Both 2D and 3D versions were published in [27] and in [25, 26, 28] respectively.

3.1 Method Overview

The ICP algorithm is effective when both range scans are already nearly aligned, otherwise, the unknown data association can lead to convergence to an incorrect local minima, where the distances between points are small enough for the algorithm to have converged, but the correspondence between the points do not match correctly. Take for instance the example shown in Fig. 3.1, where two convergence situations are presented. In the first situation, Fig. 3.1(a) and 3.1(c), the initial alignment transformation was good enough for the ICP to be able to converge to the right solution. On the contrary, Fig. 3.1(b) and 3.1(d) show an example where the ICP algorithm has converged to an incorrect local minimum due to the bad initial transformation.

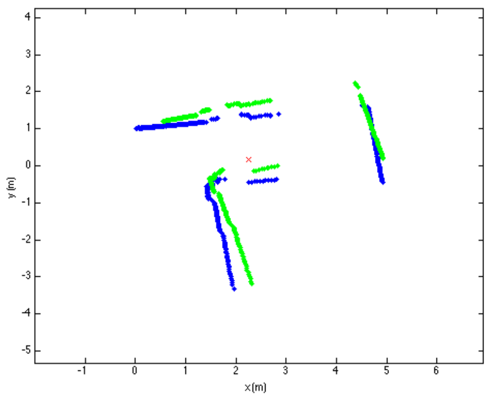

(a)

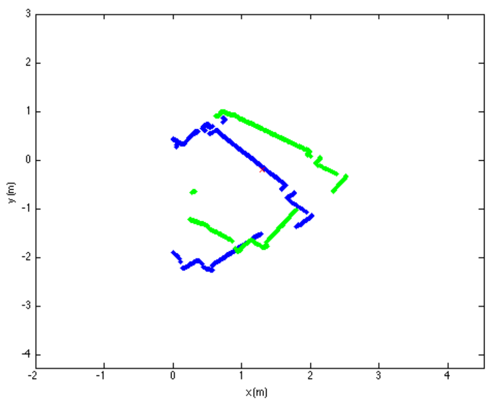

(b)

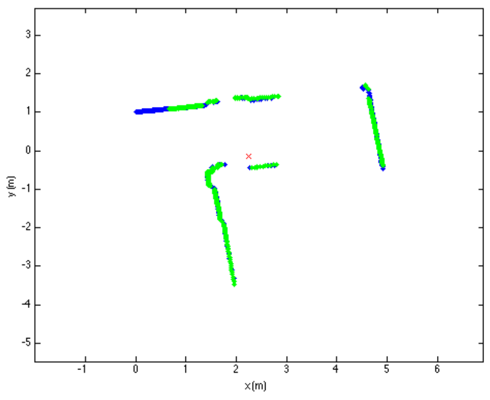

(c)

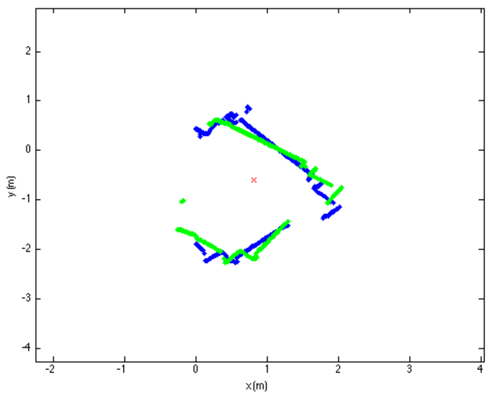

(d)

Figure 3.1: (a) and (b) are examples of two points cloud being aligned with ICP. (c) ICP converged to a correct local minimum. (d) ICP converge to an incorrect local minimum.

The ICP algorithm does not guarantee convergence to the correct local minimum, and therefore the map obtained from the alignment of consecutive pairs of frames may contain enormous errors. However, by looking closely at Fig. 3.1(d), one can clearly see how the two clouds fit together. Based on the assumption that users have the perception and capability to judge if the alignment between two scans needs to be improved, they become active players by interfering with the alignment process, providing valuable help in the improvement of the scans adjustment.

Consider two range scans, S_{i-1} and S_i, each one with N points, stored in two consecutive nodes in a graph:

$$\begin{aligned} S_{i-1} &= M = \{m_k\}, \\ S_i &= D = \{d_k\}, \\ m_k, d_k \in \mathbb{R}^2 &\text{ or } m_k, d_k \in \mathbb{R}^3 , \end{aligned}$$

and a rigid transformation in homogeneous coordinates, T_i^{i-1}, which align D with M:

$$T_i^{i-1} = \left[\begin{array}{c|c} R & t \\ \hline 0 & 1 \end{array} \right], \tag{3.1}$$

where R is a rotation matrix and t is a translation vector. This transformation can be initialized to a default value (e.g. $R = I$ and $t = 0$) or computed with an alignment algorithm (e.g. ICP). By applying this transformation to D, a transformed scan, D' is obtained. The two scans (M and D') are then presented in a viewer (GUI) for alignment analysis. Then, the user decides if M and D are correctly aligned. If yes, the next pair of scans in the graph is displayed on the interface, if not, in order to correct their alignment, the user interacts with the viewer using common computer mouse and keyboard, and apply either translations or rotations to one of the scans (D'). These actions are carried out separately using a designated key to choose which mode to use. Each time an interactive mode is used, a new transformation that align D' with M is obtained. Depending on which mode is used, we obtain transformation T_t if the mode is translations or transformation T_R if the mode is rotations. These transformations are then applied to the transformation in the graph edge corresponding to the scan pair being analysed:

$$T_i^{i-1} \leftarrow T_t \, T_i^{i-1}, \quad \text{if translation mode was used,} \tag{3.2}$$

$$T_i^{i-1} \leftarrow T_R \, T_i^{i-1}, \quad \text{if rotation mode was used.} \tag{3.3}$$

Figure 3.2 describes how the method works.

The task of manually adjusting pairs of two scans can become time consuming and sometimes tough, specially when the alignment is being performed in the 3D space, where the interaction with scans (translations and rotations) using a computer mouse is harder due to the increase of the DoF from three to six.

In order to help the user in the alignment process, this thesis proposes a force based system that restrain the movement of the scans. Scans are aligned by balancing a virtual force caused by a mouse drag, henceforth called mouse force, with a reaction force produced by a potential field.

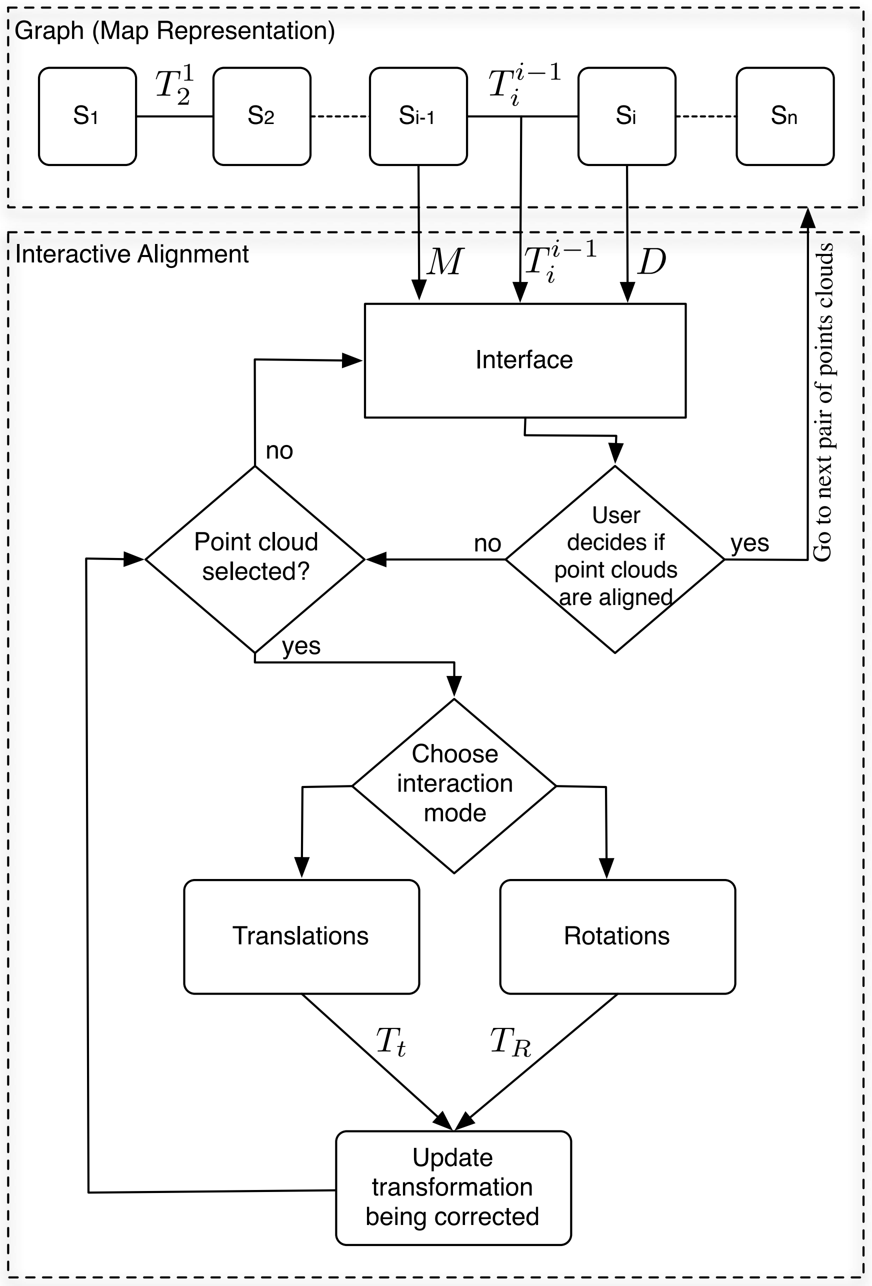

Figure 3.2: Interactive Alignment method.

3.2 Potential Functions

This section explains how the mouse and reaction forces are originated, and introduces the potential functions responsible for their creations.

3.2.1 Mouse Force

The mouse force is the force exerted by the user when he intends to move a scan. This force is created when the user clicks on one point of the scan and attempts to drag it. The drag is defined by two points in the image: p_o, the point where the user clicked, and p_f, the point corresponding to the mouse cursor current position. As said before, there are two ways of interacting with scans: translations and rotations.

In the case of translations (Fig. 3.3) the mouse force is proportional to the difference between p_f and the initial point p_o. As the scan D' moves during interaction, the scan point corresponding to p_o also moves and new positions are computed by doing:

$$p'_o = p_o + t \tag{3.4}$$

where p'_o is the point p_o translated by t.

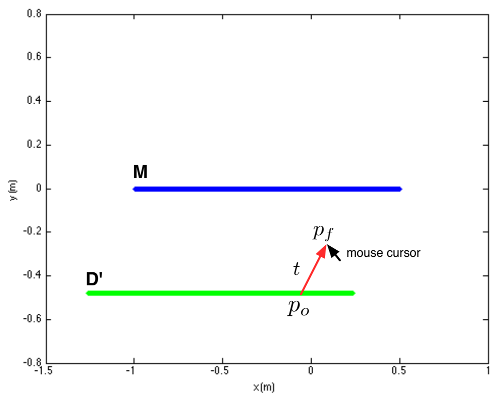

Figure 3.3: Geometry of the mouse force, originated from a mouse drag.

When performing rotations (Fig. 3.4), the mouse force is also created by dragging the point clicked by the user. However, in this case the mouse force produces a torque τ_m which makes the scan D' rotate. The rotation is performed around a rotation center c, and is defined by a rotation matrix, R.

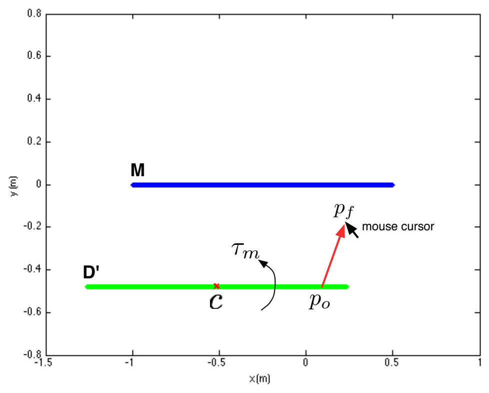

Figure 3.4: Torque produced by force originated from a mouse drag

Like translations, while D' moves, the new positions of p_o are given by:

$$p'_o = R(\theta)(p_o - c) + c, \tag{3.5}$$

where c is the rotation center.

In the general case, the movement of scan D' is defined by a rigid transformation defined by a rotation matrix R, a rotation center c and a translation t. Point p_o is transformed into $p'_o = R\,(p_o - c) + c + t$. The potential function, J_m, that grows with the distance between points p'_o and p_f is defined as follows:

$$J_m = \frac{1}{2}\|p_f - p'_o\|^2. \tag{3.6}$$

By taking the gradient of this potential, with respect to either translation t and rotation R, one obtains the virtual forces and torques induced by the mouse drag:

$$F_m = -k_m\, \nabla_t\, J_m, \tag{3.7}$$

$$\tau_m = -k_m\, \nabla_R\, J_m, \tag{3.8}$$

where F_m and τ_m are the force and the torque produced by a mouse drag respectively and k_m is a proportionality constant.

3.2.2 Reaction Force

Opposing the mouse force, is the reaction force which is produced by a potential field. This potential field is defined by threshold ξ_{pot}, which creates a region of actuation that makes any scan that enters in it, be automatically attracted towards M (Fig. 3.5).

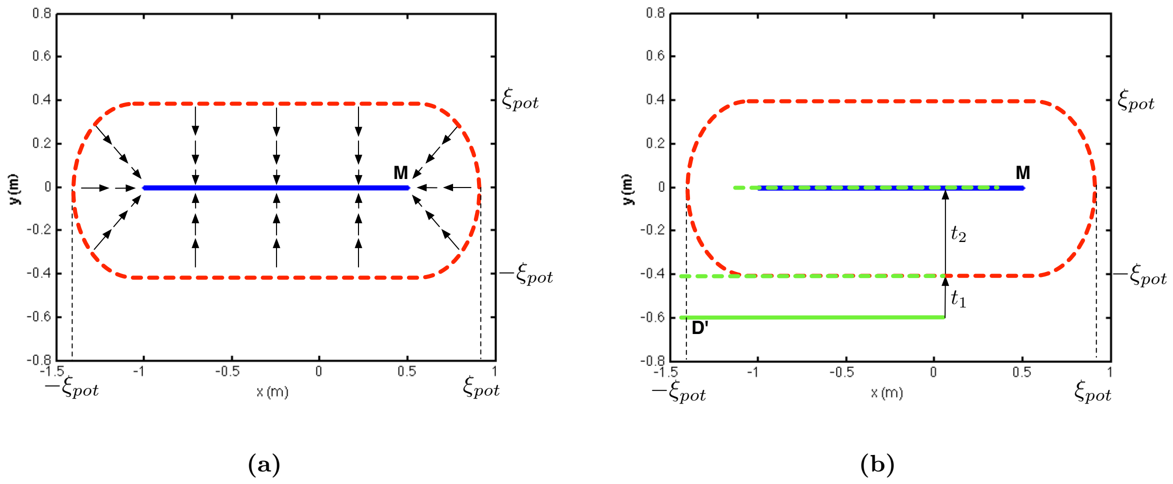

Figure 3.5: (a) Potential field of scan M. (b) Reaction force example.

Two scans are attracted to each other by minimizing the distance between corresponding points. Similarly to ICP algorithm, this minimization consists in computing the best rigid transformation that aligns D' with M. For instance, in Fig 3.5(b) a translation t_1 is applied to D' towards M, and as soon as D' comes in contact with the potential field, points from D' are paired with the closest points of M, producing the reaction force that makes the scan D' attract towards M. The closest points are computed in the same fashion as in ICP (using a Kd-tree), and only points that are within the threshold are considered. These pairs are then used to compute the rigid transformation that better align both scans. The potential function that minimizes the distance between pairs of corresponding points is given by:

$$J_r = \frac{1}{2}\sum_{k=1}^{N} \|m_k - [R\,(d_k - c) + c + t]\,\|^2, \tag{3.9}$$

where $[m_k, d_k]$ are pairs of closest points from M to D', and N is the number of these pairs. This function is similar to the potential cost function ICP, with the difference of rotations being performed about a center of rotation rather than around the origin.

The reaction forces and torques induced by the mouse drag can be obtained bytaking the gradient of this potential, with respect to either translation t and rotation R:

$$F_r = -k_r\,\nabla_t\,J_r, \tag{3.10}$$

$$\tau_r = k_r\,\nabla_R\,J_r, \tag{3.11}$$

where F_r and τ_r are the force and the torques induced by the mouse drag respectively and k_r is a proportionality constant.

3.3 Alignment in 2D

This section addresses the two interactive modes which users can use to interact with scans ("Translations" and "Rotations" blocks from Fig. 3.2) and makes use of the two forces described before to derive the expressions used to compute the translations and the rotation angles in the 2D space.

3.3.1 Translations

In this mode, the alignment consists in a translation by t. Thus R is the identity, and the potential functions (3.6) and (3.9) are simplified to:

$$J_m|_{R=I} = \frac{1}{2}\|p_f - (p_o + t)\,\|^2, \tag{3.12}$$

$$J_r|_{R=I} = \frac{1}{2}\sum_{k=1}^{N} \|m_k - (d_k + t)\,\|^2. \tag{3.13}$$

The mouse force F_m is computed from the gradient of the potential function (3.12) with respect to the translation t:

$$F_m = -k_m\,\nabla_t\,J_m|_{R=I}\,. \tag{3.14}$$

Opposing this force, a reaction force F_r is computed from the gradient of the potential function (3.13) with respect to the translation t:

$$F_r = -k_r\,\nabla_t\,J_r|_{R=I}\,. \tag{3.15}$$

The forces can be trivially computed by using the vector derivatives rules to compute the gradients of (3.14) and (3.15):

$$F_m = k_m\,[p_f - (p_o + t)]\,, \tag{3.16}$$

$$F_r = k_r\sum_{k=1}^{N}[m_k - (d_k + t)]\,. \tag{3.17}$$

To find a scan adjustment that balances the mouse and the reaction forces, translations are iteratively performed, since each time scan D' moves, the correspondences among points may change. So, for each iteration, a translation t is computed by solving the equation

$$F_m + F_r = 0, \tag{3.18}$$

with respect to t. This equation has the following algebraic closed form solution:

$$t = \frac{k_m(p_f - p_o) + k_r \sum_{k=1}^{N}(m_k - d_k)}{k_m + Nk_r}. \tag{3.19}$$

Algorithm 3.1 Compute Translation

```
function TRANSLATION($p_o, p_f, M, D'$)
    $D_{new} \leftarrow D'$
    repeat
        $P \leftarrow ComputeClosestPoints(M, D_{new})$
        $t \leftarrow ComputeTranslation(p_o, p_f, P)$
        $D_{new} \leftarrow UpdateScan(D', t)$
    until $ErrorChange(t) < \xi_t$
    return $t$
end function
```

The scan adjustment results from the algorithm 3.1. The algorithm receives the mouse initial and current position and the two scans being adjusted (M and D') as input. The algorithm starts by computing a subset, P, of pairs of closest points from the two scans ($P \subset \{[m_1, d_1]...[m_k, d_k]\}$) The subset P is then used together with the mouse positions in (3.19) to compute the translation. Finally scan D' is updated with the new estimate of the translation and the convergence is checked. The algorithm iterates until the correspondences between points are the same, or in other words until the norm of the difference between the new and the previous translation estimation falls below a threshold:

$$\|t_i - t_{i-1}\| < \xi_t, \tag{3.20}$$

where t_{i-1} and t_i are the estimation of the translation at iteration $i-1$ and i respectively and ξ_t is a threshold.

The obtained $t = [t_x\ t_y]^T$ corresponds to the homogeneous transformation:

$$T_t = \left[\begin{array}{c|c} I_{2\times 2} & t \\ \hline 0 & 1 \end{array}\right], \tag{3.21}$$

where $I_{2\times 2}$ is a 2×2 identity matrix.

Figure 3.6 shows an example of two scans being align by applying translations, with and without forces. On the left three sub-figure, scan D' (green) moves freely (mouse current position is the same as the initial point clicked), due to the absence of the potential field. On the contrary, on the other three sub-figures the balance of the forces (F_m and F_r) restrain the movement of the scan by favouring the adjustment along the corridor, while disfavouring movements orthogonal to the corridor.

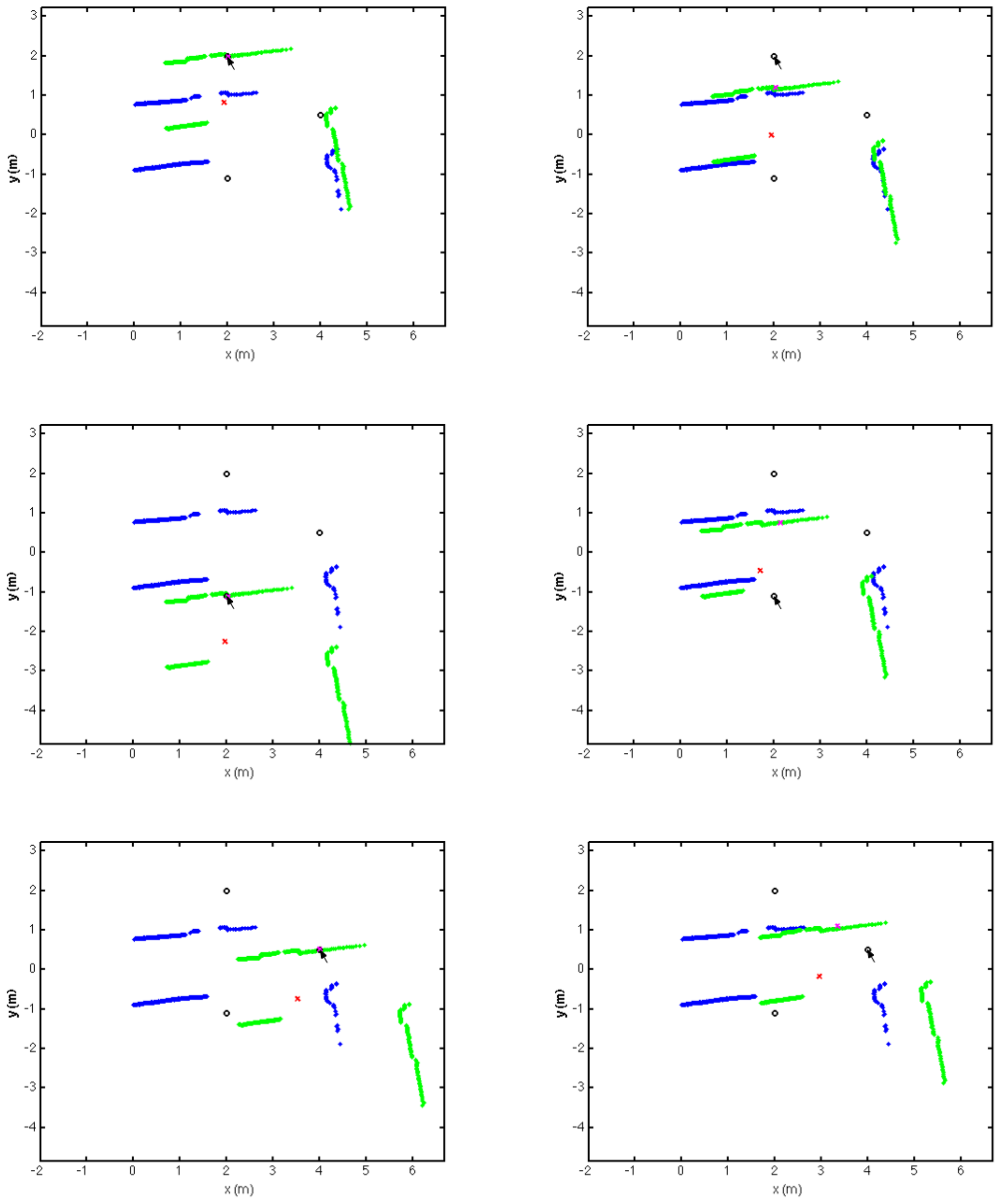

Figure 3.6: Two corridors being aligned using translations as interactive mode. Left three figures: alignment without forces. Right three figures: alignment with forces. Black arrow is the mouse current position, the magenta "x" is the initial point clicked, the red "x" is the scan centroid and the back "O" are references points used only for analysis purposes. Results obtained using $k_m = 0.2$, $k_r = 0.002$, $\xi_t = 0.01m$ and $\xi_{pot} = 0.4m$.

3.3.2 Rotations

In the Euclidean space, the rotation of one point in the xy-Cartesian plane through an angle θ about the origin, can be performed using the usual rotation matrix:

$$R(\theta) = \begin{bmatrix} \cos(\theta) & -\sin(\theta) \\ \sin(\theta) & \cos(\theta) \end{bmatrix}. \tag{3.22}$$

Rotation mode comprises a rotation of scan D', with respect to the center of mass c, by an angle θ (Fig. 3.4). The center of mass of a scan is set to its centroid. When the user clicks on the scan D' and attempts to drag it, a force F_m is created using (3.6), for $t = 0$. The cost functions (3.6) and (3.9) are simplified to:

$$\begin{aligned} J_m|_{t=0} &= \frac{1}{2}\|p_f - [R(\theta)\ (p_o - c) + c]\|^2 \\ &= \frac{1}{2}\|p'_f - R(\theta)\ r_i)\|^2, \end{aligned} \tag{3.23}$$

$$\begin{aligned} J_r|_{t=0} &= \frac{1}{2}\sum_{k=1}^{N} \|m_k - [R(\theta)\ (d_k - c) + c]\|^2 \\ &= \frac{1}{2}\sum_{k=1}^{N} \|m'_k - R(\theta)\ d'_k\|^2, \end{aligned} \tag{3.24}$$

where $r_i = (p_o - c)$, $p'_f = (p_f - c)$, $m'_k = (m_k - c)$ and $d'_k = (d_k - c)$.

However, unlike translations, the balance is formulated here in terms of virtual torques. The mouse torque τ_m is the gradient of the cost function (3.23) with respect to θ:

$$\tau_m = -k_m\, \nabla_\theta\ J_m|_{t=0}\,. \tag{3.25}$$

The opposing torque τ_r is the gradient of the cost function (3.24) with respect to θ:

$$\tau_r = -k_r\, \nabla_\theta\ J_r|_{t=0}\,. \tag{3.26}$$

Both gradients can be computed using the chain rule:

$$\nabla_\theta\ J_m|_{t=0} = tr\left[\left(\frac{\partial J_m}{\partial R(\theta)}\right)^T \frac{\partial R(\theta)}{\partial \theta}\right], \tag{3.27}$$

$$\nabla_\theta\ J_r|_{t=0} = tr\left[\left(\frac{\partial J_r}{\partial R(\theta)}\right)^T \frac{\partial R(\theta)}{\partial \theta}\right], \tag{3.28}$$

and the partial derivatives can be trivially obtained using the matrix and vector derivative rules:

$$\frac{\partial J_m}{\partial R(\theta)} = -p'_f r_i^T, \tag{3.29}$$

$$\frac{\partial J_r}{\partial R(\theta)} = -\sum_{k=1}^{N} m'_k (d'_k)^T, \tag{3.30}$$

$$\frac{\partial R(\theta)}{\partial \theta} = \begin{bmatrix} -\sin(\theta) & -\cos(\theta) \\ \cos(\theta) & -\sin(\theta) \end{bmatrix} = AR(\theta), \tag{3.31}$$

where $A = \begin{bmatrix} 0 & -1 \\ 1 & 0 \end{bmatrix}$.

Both torques are obtained by computing the trace of (3.27) and (3.28) and using the partial derivatives from (3.29), (3.30) and (3.31) :

$$\tau_m = k_m r_i^T R^T A^T p'_f, \tag{3.32}$$

$$\tau_r = k_r \sum_{k=1}^{N} (d'_k)^T R^T A^T m'_k. \tag{3.33}$$

As in the case of translations, the scan D' is iteratively rotated until convergence of the correspondences is reached. In each iteration, the balance of torques

$$\tau_m + \tau_r = 0 \tag{3.34}$$

has a closed form solution. Using (3.32) and (3.33) in (3.34) we can obtain

$$\tan(\theta) = \frac{k_m r_i^T A^T p'_f + k_r \sum_{k=1}^{N} (d'_k)^T A^T m'_k}{k_m r_i^T p'_f + k_r \sum_{k=1}^{N} (d'_k)^T m'_k}. \tag{3.35}$$

However, this only allows us to compute θ up to a π congruence. To resolve this ambiguity, which is caused by the existence of two solutions π radians appart, one has to determine which one corresponds to a stable solution. This can be easily determined from the sign of the derivative of the total torque $\tau = \tau_m + \tau_r$:

$$\frac{\partial \tau}{\partial \theta} = -k_m r_i^T R^T(\theta) p'_f - k_r \sum_{k=1}^{N} (d'_k)^T R^T(\theta)\, m'_k. \tag{3.36}$$

A solution is stable if and only if the sign of this derivative is negative. A positive derivative implies that a small perturbation in θ will swing the scan π radians towards the other solution. Note that (3.36) has opposite signs for angles θ and $\theta + \pi$, and therefore there is always a single negative solution.

Algorithm 3.2 Compute Rotation Angle

```
function ROTATIONS($p_o, p_f, M, D'$)
    $c \leftarrow ComputeScanCentroid(D')$
    $D_{new} \leftarrow D'$
    $r_i \leftarrow p_o - c$
    $p'_f \leftarrow p_f - c$
    repeat
        $P \leftarrow ComputeClosestPoints(M, D_{new})$
        for each pair of closest points in $P$ do
            $m'_k \leftarrow m_k - c$
            $d'_k \leftarrow d_k - c$
            $P' \leftarrow (m'_k, d'_k)$
        end for
        $\theta \leftarrow ComputeRotationAngle(r_i, p'_f, P')$
        if $sign(ComputeTorqueDerivative(\theta, r_i, p'_f, P')) > 0$ then
            $\theta \leftarrow \theta + \pi$
        end if
        $D_{new} \leftarrow UpdateScan(D', \theta)$
    until $ErrorChange(\theta) < \xi_\theta$
    return $\theta$
end function
```

Algorithm 3.2 shows the steps needed to adjust the scans when performing rotations. The algorithm starts by computing the scan centroid and used it to center the mouse positions in the origin. In each iteration, new correspondences are obtained and used to compute the rotation angle. The stable solution is then chosen using (3.36). Finally scan D' is updated with the new estimate of the rotation angle and the convergence is checked. The algorithm iterates until the module of the difference between the new and the previous rotation angle falls below a threshold:

$$|\theta_i - \theta_{i-1}| < \xi_\theta, \tag{3.37}$$

where θ_{i-1} and θ_i are the estimation of the rotation angle at iteration $i-1$ and i respectivelyand ξ_θ is a threshold.

A rotation transformation is then created using the value θ,

$$T_R = \begin{bmatrix} \cos(\theta) & -\sin(\theta) & b_x \\ \sin(\theta) & \cos(\theta) & b_y \\ 0 & 0 & 1 \end{bmatrix}, \tag{3.38}$$

$$b = \begin{bmatrix} b_x \\ b_y \end{bmatrix} = [I - R(\theta)]\, c. \tag{3.39}$$

Note that translation b accounts for the fact that the rotation is performed with respect to center c, rather than to the origin.

Figure 3.7 shows an example of two scans being align by applying rotations, without using forces and using forces. As it can be seen, the balance of the two torques is able to restrain the movement of the scans.

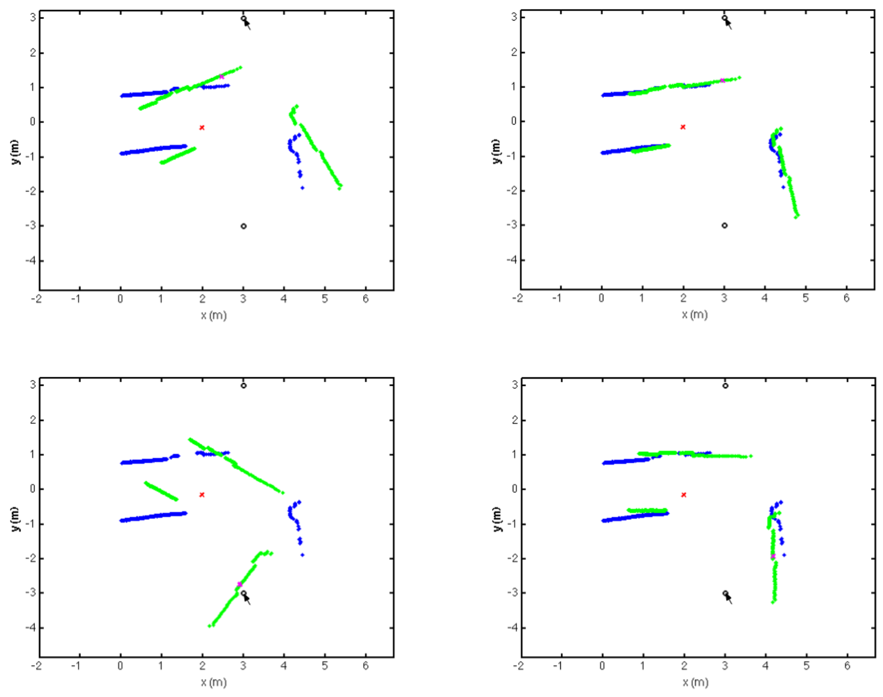

Figure 3.7: Two corridors being aligned using rotations. Left two figures: alignment without forces. Right two figures: alignment with forces. Black arrow is the mouse current position, the magenta "x" is the initial point clicked, the red "x" is the point cloud center of mass and the back "O" are references points used only for analysis purposes. Results obtained using $k_m = 0.1$, $k_r = 0.004$, $\xi_\theta = 0.01m$ and $\xi_{pot} = 0.4m$

3.4 Extension to 3D

This section extends the proposed method to the 3D space. The algorithm and the potential functions presented in section 3.1 and 3.2 remain the same. The only thing that changes is the way block "Translations" and "Rotations" from Fig. 3.2 are implemented. Contrary to what happens in the 2D space, in the 3D space the interaction with point clouds using a computer mouse becomes harder due the increase of the DoF from three to six. Using a computer mouse, one can only control two DoF, so the interaction between users and point clouds is restricted to a plane parallel to the image plane. Translation and rotations are performed using mouse forces defined on this plane.

Performing rotations in 3D with a computer mouse is not a trivial task, so the user is allowed to choose among tree types of rotations, based on previous studies concerning human-computer interaction with 3D objects:

1. Rotation without restrictions: in this mode the three DoF are taken into account when computing the rotations matrix (see section 3.4.2);
2. Rotation restrict to a plane (see [22]): in this mode rotations are performed around an axis orthogonal to the plane parallel to the image plane (see section 3.4.3.A);
3. Rotation using a virtual sphere (see [23]): in this mode the point clicked is projected onto the image plane and used alongside the mouse current position in the image plane to compute the rotation axis and the angle each time the mouse moves (see section 3.4.3.B).

3.4.1 Translations

In 3D, we only have access to the coordinates of the pixel of the mouse current position in the image plane, therefore the mouse force is defined on a 3D plane parallel to the image plane. The drag is defined by two 3D points, p_o and p_f, corresponding to the initial and final drag points. When the user clicks on point could D', the initial point p_o is set to the point on D' which projection on the image plane is closest to the mouse point clicked by the user. As the user drags the mouse, p_f is defined by the projection of the new mouse point onto the plane parallel to the image plane that crosses p_o (Fig. 3.8). As point cloud D' moves during interaction, the point corresponding to p_o also moves.

The mouse force, produced by a mouse drag, is obtained using p_o and p_f in the potential function (3.6), and by computing its gradient with respect to the translation t, when there is no rotation, $R = I_{3\times3}$. The result obtained is the same as (3.16).

The reaction force is also obtained by computing the gradient of the potential function (3.9) with respect to the translation t when the rotation $R = I_{3\times3}$. The closest points ($\{m_k\}$ and $\{d_k\}$) are computed in the same way as in ICP (Kd-trees) and only the pairs sufficiently close are considered. The result obtained is the same as (3.17).

By balancing the two forces, $F_m + F_r = 0$, we obtain the same close form solution as the one obtained for translations (3.19) in the 2D space.

The scan adjustment follows the same algorithm as the one described in section 3.3.1. The only difference is the way p_o and p_f are obtained.

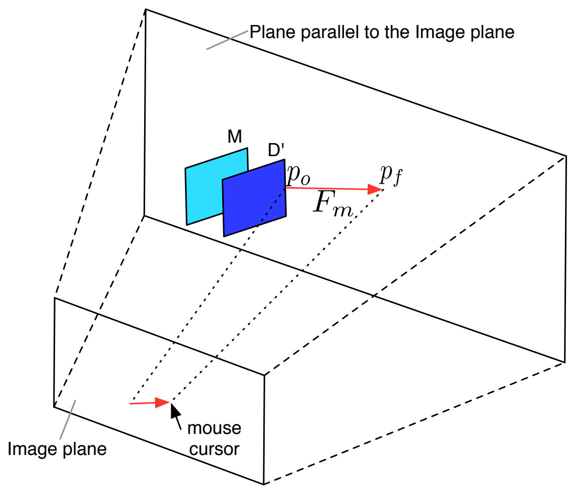

Figure 3.8: 3D representation of the mouse force, defined by p_o and p_f. Force is applied to point cloud D'.

In the end of the algorithm, the obtained $t = [t_x\ t_y\ t_z]^T$ corresponds to the homogeneous transformation:

$$T_t = \left[\begin{array}{c|c} I_{3\times3} & t \\ \hline 0 & 1 \end{array}\right]. \tag{3.40}$$

3.4.2 Unrestricted Rotations

As in the case of 2D rotations, in the 3D space, point clouds are also rotated with respect to their center of mass c. The center of mass of the point cloud is set to its centroid.

In three dimensions the rotation around each axis, x, y and z, can be performed using the following rotation matrices respectively:

$$R_x(\alpha) = \begin{bmatrix} 1 & 0 & 0 \\ 0 & \cos(\alpha) & -\sin(\alpha) \\ 0 & \sin(\alpha) & \cos(\alpha) \end{bmatrix} \qquad R_y(\beta) = \begin{bmatrix} cos(\beta) & 0 & \sin(\beta) \\ 0 & 1 & 0 \\ -\sin(\beta) & 0 & \cos(\beta) \end{bmatrix} \qquad R_z(\gamma) = \begin{bmatrix} \cos(\gamma) & -\sin(\gamma) & 0 \\ \sin(\gamma) & \cos(\gamma) & 0 \\ 0 & 0 & 1 \end{bmatrix}, \tag{3.41}$$

where α, β and γ are the Euler angles. A Rotation matrix, $R(\alpha, \beta, \gamma)$, can then be written as a multiplication of $R_x(\alpha)$, $R_y(\beta)$ and $R_z(\gamma)$. In this thesis the following order was used:

$$R(\alpha, \beta, \gamma) = R_z(\gamma)\ R_y(\beta)\ R_x(\alpha) \tag{3.42}$$

which means that the rotation is first made around axis x, then around axis y and finally around axis z (see [43] for review about 3D rotations).

When the user clicks on the point cloud D' and attempts to drag it, a force F_m is created using (3.6), for $t = 0$ and $R = R(\alpha, \beta, \gamma)$. Like 2D rotations, the force balance here is also formulated in terms of virtual torques.

The mouse torque τ_m is the gradient of the cost function (3.6) computed around rotation R. Infinitesimal rotations α, β and γ, along axis x, y, and z are considered.

$$\tau_m = -k_m\, \nabla_{\alpha,\beta,\gamma}\ J_m|_{t=0,\alpha=\beta=\gamma=0}\,. \tag{3.43}$$

The opposing torque τ_r is the gradient of the cost function (3.9) with respect to α, β and γ:

$$\tau_r = -k_r\, \nabla_{\alpha,\beta,\gamma}\ J_r|_{t=0,\alpha=\beta=\gamma=0}\,. \tag{3.44}$$

Note that Euler angles suffer from singularities, however, the rotation is parametrized using a rotation matrix, while the Euler angles are only used for computing derivatives(small angle approximation). Thus, derivatives in (3.43) and (3.44) are done around the point $\alpha = 0$, $\beta = 0$ and $\gamma = 0$.

Both gradients can be computed using the chain rule:

$$\nabla_{\alpha,\beta,\gamma}\, J_m|_{t=0,\alpha=\beta=\gamma=0} = \left[tr\left[\left(\frac{\partial J_m}{\partial R(\alpha,\beta,\gamma)}\right)^T \frac{\partial R(\alpha,\beta,\gamma)}{\partial x}\right]\right], \tag{3.45}$$

$$\nabla_{\alpha,\beta,\gamma}\, J_r|_{t=0,\alpha=\beta=\gamma=0} = \left[tr\left[\left(\frac{\partial J_r}{\partial R(\alpha,\beta,\gamma)}\right)^T \frac{\partial R(\alpha,\beta,\gamma)}{\partial x}\right]\right], \tag{3.46}$$

where $x = \alpha$, β and γ.

The partial derivative $\frac{\partial R(\alpha,\beta,\gamma)}{\partial x}$ can be computed using the derivative definition:

$$\frac{\partial R(\alpha,\beta,\gamma)}{\partial x} = \lim_{x\to 0} \frac{R(x_0 + x) - R(x_0)}{x} = \lim_{x\to 0}\frac{(R(x) - I)\, R(x_0)}{x} = A_x R(x_0), \tag{3.47}$$

where $x_0 = (\alpha, \beta, \gamma)$,

$$A_\alpha = \begin{bmatrix} 0 & 0 & 0 \\ 0 & 0 & -1 \\ 0 & 1 & 0 \end{bmatrix},\ A_\beta = \begin{bmatrix} 0 & 0 & 1 \\ 0 & 0 & 0 \\ -1 & 0 & 0 \end{bmatrix} \text{ and } A_\gamma = \begin{bmatrix} 0 & -1 & 0 \\ 1 & 0 & 0 \\ 0 & 0 & 0 \end{bmatrix}.$$

The partial derivative $\frac{\partial J_m}{\partial R(\alpha,\beta,\gamma)}$ and $\frac{\partial J_r}{\partial R(\alpha,\beta,\gamma)}$ can be trivially obtained by computing the derivative of expression (3.6) and (3.9) with respect to $R(\alpha,\beta,\gamma)$, which has the same result as (3.29) and (3.30):

$$\frac{\partial J_m}{\partial R(\alpha,\beta,\gamma)} = -p'_f r_i^T, \tag{3.48}$$

$$\frac{\partial J_r}{\partial R(\alpha,\beta,\gamma)} = -\sum_{k=1}^{N} m'_k (d'_k)^T. \tag{3.49}$$

Using the results (3.48), (3.49) and (3.47) in (3.45) and (3.46), it is possible to write the expression of the torques:

$$\tau_m = -k_m \left[tr\left[r_i \left(p'_f\right)^T A_x R\right]\right], \tag{3.50}$$

$$\tau_r = -k_r \left[tr\left[\sum_{k=1}^{N} d'_k \left(m'_k\right)^T A_x R\right]\right], \tag{3.51}$$

where $x = \alpha$, β and γ. Note that the rotation, R, is parametrized using a rotation matrix so:

$$R = \begin{bmatrix} r_{11} & r_{12} & r_{13} \\ r_{21} & r_{22} & r_{23} \\ r_{31} & r_{32} & r_{33} \end{bmatrix} \tag{3.52}$$

where

$$R^T R = I \text{ and } det(R) = 1 \tag{3.53}$$

Similarly to 2D rotations, the objective here is also to find the rotation, R, that balances the torques :

$$\tau_m + \tau_r = 0. \tag{3.54}$$

Using the result from (3.50) and (3.51) in (3.54) and using the trace properties, three equation are obtained:

$$\mathrm{tr}\left[\left(k_m r_i \left(p'_f\right)^T + k_r \sum_{k=1}^{N} d'_k \left(m'_k\right)^T\right) A_x R\right] = 0, \tag{3.55}$$

where $x = \alpha$, β and γ. The nine unknown variables referred in (3.52) can be obtained by solving the non-linear system composed by the three equations in (3.55) and the six equations from the constrain (3.53):

$$\begin{aligned}
&b_{13}r_{21} + b_{23}r_{22} + b_{33}r_{23} - b_{12}r_{31} - b_{22}r_{32} - b_{32}r_{33} = 0,\\
&-b_{13}r_{11} - b_{23}r_{12} - b_{33}r_{13} + b_{11}r_{31} - b_{21}r_{32} + b_{31}r_{33} = 0,\\
&b_{12}r_{11} + b_{22}r_{12} + b_{32}r_{13} - b_{11}r_{21} - b_{21}r_{22} - b_{31}r_{23} = 0,\\
&r_{11}^2 + r_{21}^2 + r_{31}^2 = 1,\\
&r_{12}^2 + r_{22}^2 + r_{32}^2 = 1,\\
&r_{13}^2 + r_{23}^2 + r_{33}^2 = 1,\\
&r_{11}r_{12} + r_{21}r_{22} + r_{31}r_{32} = 0,\\
&r_{11}r_{13} + r_{21}r_{23} + r_{31}r_{33} = 0,\\
&r_{12}r_{13} + r_{22}r_{23} + r_{32}r_{33} = 0,
\end{aligned} \tag{3.56}$$

where

$$B = \begin{bmatrix} b_{11} & b_{12} & b_{13} \\ b_{21} & b_{22} & b_{23} \\ b_{31} & b_{32} & b_{33} \end{bmatrix} = k_m r_i \left(p'_f\right)^T + k_r \sum_{k=1}^{N} d'_k \left(m'_k\right)^T .$$

The point cloud D' is iteratively rotated until convergence of the correspondences is reached. In each iteration, balancing the torques consists in solving the above system. Due to the non-linearity of the system, a suitable solver[1] is used to resolve (3.56).

Algorithm 3.3 summarizes the steps needed to perform the point clouds adjustment. The algorithm framework is similar to the one in 2D rotations. The way points p_o and p_f are obtained and the condition to check the convergence (*ErrorChange*) are the only changes.

Algorithm 3.3 Compute Rotation Matrix

```
function UnrestrictedRotation($p_o, p_f, M, D'$)
    $c \leftarrow ComputeScanCentroid(D')$
    $D_{new} \leftarrow D'$
    $r_i \leftarrow p_o - c$
    $p'_f \leftarrow p_f - c$
    repeat
        $P \leftarrow ComputeClosestPoints(M, D_{new})$
        for each pair of closest points in $P$ do
            $m'_k \leftarrow m_k - c$
            $d'_k \leftarrow d_k - c$
            $P' \leftarrow (m'_k, d'_k)$
        end for
        $R \leftarrow ComputeRotationMatrix(r_i, p'_f, P')$
        $D_{new} \leftarrow UpdateScan(D', R)$
    until $ErrorChange(R) < \xi_R$
    return $R$
end function
```

The balanced of the forces is achieved when the difference between the rotation angle computed in iteration $i - 1$ and i falls below a threshold ξ_R. The angular difference can be obtained from the

[1]A variation of the Levenberg Marquardt algorithm was used, as implemented in Eigen library (http://eigen.tuxfamily.org, online on 10-Oct-2012).

incremental rotation between two consecutive iterations:

$$R_i^{i-1} = R_{i-1}\, R_i^{-1}, \tag{3.57}$$

where R_i^{i-1} is the incremental rotation and R_{i-1} and R_i are the rotations computed in iteration $i-1$ and i respectively. The angular difference, δ, is computed using the following expression (see [43]):

$$\delta = \cos^{-1}\left(\frac{\operatorname{tr}\left(R_i^{i-1}\right) - 1}{2}\right). \tag{3.58}$$

The loop ends when the following condition is met

$$|\delta| < \xi_R. \tag{3.59}$$

After exiting the loop, a rotation transformation is then created using the matrix R computed and used to create the final homogeneous transformation, T_R:

$$T_R = \left[\begin{array}{c|c} R & b \\ \hline 0 & 1 \end{array}\right], \tag{3.60}$$

$$b = \begin{bmatrix} b_x \\ b_y \\ b_z \end{bmatrix} = [I - R]\, c. \tag{3.61}$$

Note that translation b accounts for the fact that the rotation is performed with respect to center c, rather than to the origin.

3.4.3 Restricted Rotations

Restricted rotations are an alternative way of performing rotations in the 3D space. They consist in rotating a point cloud by an angle θ, around an axis of rotation u, centered in a center of mass c (Fig. 3.9).

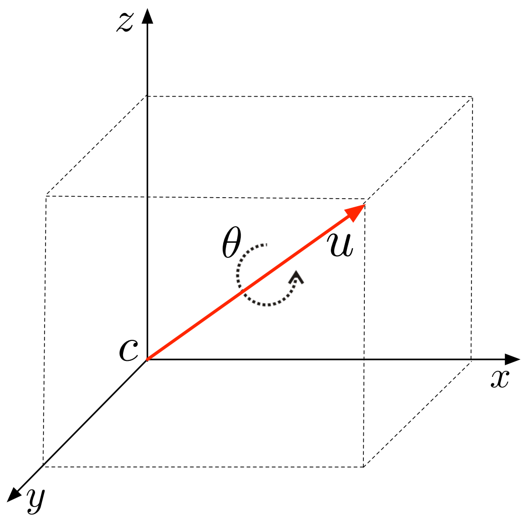

Figure 3.9: Geometry of the axis of rotation u and the angle of rotation θ.

The DoF are reduced from three to one. The rotation matrix is given by the Rodrigues' rotation formula, which says that given an unit vector $u = [u_x, u_y, u_z]$, where $u_x^2 + u_y^2 + u_z^2 = 1$, the matrix which performs a rotation by an angle θ about an axis in the direction of u is:

$$R(\theta) = I\cos(\theta) + \sin(\theta)\, U_1 + (1 - \cos(\theta))\, U_2, \tag{3.62}$$

where

$$U_1 = \begin{bmatrix} 0 & -u_z & u_y \\ u_z & 0 & -u_x \\ -u_y & u_x & 0 \end{bmatrix} \text{ and } U_2 = \begin{bmatrix} u_x^2 & u_x u_y & u_x u_z \\ u_x u_y & u_y^2 & u_y u_z \\ u_x u_z & u_y u_z & u_z^2 \end{bmatrix}.$$

There are several axis of rotation that can be used to rotate point clouds around them. Two particular rotations, described in section 3.4.3.A and 3.4.3.B, can be implemented using different methods to compute this axis. Once computed, vector u needs to be normalized to meet the constrain $u_x^2 + u_y^2 + u_z^2 = 1$:

$$u = \frac{u}{\|u\|}. \tag{3.63}$$

When the user clicks on the point cloud D' and attempts to drag it, a force F_m is created using (3.6), for $t = 0$ and $R = R(\theta)$. The expressions of the torques are very similar to the ones derived in 2D rotations. The mouse torque τ_m is the gradient of the potential function (3.6) with respect to θ:

$$\tau_m = -k_m \nabla_\theta\, J_m\big|_{t=0}, \tag{3.64}$$

and the opposing torque τ_r is the gradient of the potential function (3.9) with respect to θ:

$$\tau_r = -k_r \nabla_\theta\, J_r\big|_{t=0}. \tag{3.65}$$

Both gradients can be computed using the chain rule:

$$\nabla_\theta\, J_m\big|_{t=0} = tr\left[\left(\frac{\partial J_m}{\partial R(\theta)}\right)^T \frac{\partial R(\theta)}{\partial \theta}\right], \tag{3.66}$$

$$\nabla_\theta\, J_r\big|_{t=0} = tr\left[\left(\frac{\partial J_r}{\partial R(\theta)}\right)^T \frac{\partial R(\theta)}{\partial \theta}\right]. \tag{3.67}$$

The partial derivative $\frac{\partial R(\theta)}{\partial \theta}$ can be computed by making the derivative of (3.62) with respect to θ:

$$\frac{\partial R(\theta)}{\partial \theta} = U_1 \cos(\theta) - (I - U_2)\sin(\theta). \tag{3.68}$$

The partial derivatives $\frac{\partial J_m}{\partial R(\theta)}$ and $\frac{\partial J_r}{\partial R(\theta)}$ have the same result as (3.29) and (3.30) respectively, differing only on $p_o, r_i, m_k, d_k \in R^3$, $m'_k = m_k - c$ and $d'_k = d_k - c$.

The value of the torques can be obtained using (3.29), (3.30) and (3.68) in (3.66) and (3.67):

$$\begin{aligned} \tau_m &= -k_m \left[r_i^T U_1^T p'_f \cos(\theta) - r_i^T (I - U_2)^T p'_f \sin(\theta)\right], & (3.69) \\ \tau_r &= -k_r \sum_{k=1}^{N} \left[(d'_k)^T U_1^T m'_k \cos(\theta) - (d'_k)^T (I - U_2)^T m'_k \sin(\theta)\right], & (3.70) \end{aligned}$$

where N is the number of pair of closest points.

The balance of torques, $\tau_m + \tau_r = 0$, can be computed using (3.69) and (3.70), which results in the following closed form solution:

$$\tan(\theta) = \frac{k_m r_i^T U_1^T p_f' + k_r \sum_{k=1}^{N} (d_k')^T U_1^T m_k'}{k_m r_i^T U_2' p_f' + k_r \sum_{k=1}^{N} (d_k')^T U_2' m_k'}, \tag{3.71}$$

where $U_2' = (I - U_2)^T$. As happens in 2D rotations, this only allows us to compute θ up to a π congruence. As mentioned before, the stable solution corresponds to angle that makes the derivative of the total torque $\tau = \tau_m + \tau_r$ negative (refer to section 3.3.2 for full explanation):

$$\frac{\partial \tau}{\partial \theta} = -H_1 \cos\theta - H_2 \sin\theta, \tag{3.72}$$

where

$$\begin{aligned} H_1 &= k_m r_i^T U_2' p_f' + k_r \sum_{k=1}^{N} (d_k')^T U_2' m_k', && (3.73) \\ H_2 &= k_m r_i^T U_1^T p_f' + k_r \sum_{k=1}^{N} (d_k')^T U_1^T m_k'. && (3.74) \end{aligned}$$

Note that in this case, expression (3.72) also has opposite signs for angles θ and $\theta + \pi$, which makes a single negative solution always available.

The point cloud adjustment, presented in algorithm 3.4, is based on a similar algorithm to the one used in the 2D rotations. It only differs in the way p_o and p_f are obtained plus the addition of the step to compute the axis of rotation before the main loop (*ComputeAxisOfRotation*).

Algorithm 3.4 Compute restricted rotation angle

```
function RestrictedRotation($p_o, p_f, M, D'$)
    $c \leftarrow ComputeScanCentroid(D')$
    $u \leftarrow ComputeAxisOfRotation(p_o, p_f, c)$
    $D_{new} \leftarrow D'$
    $r_i \leftarrow p_o - c$
    $p_f' \leftarrow p_f - c$
    repeat
        $P \leftarrow ComputeClosestPoints(M, D_{new})$
        for each pair of closest points in $P$ do
            $m_k' \leftarrow m_k - c$
            $d_k' \leftarrow d_k - c$
            $P' \leftarrow (m_k', d_k')$
        end for
        $\theta \leftarrow ComputeRotationAngle(u, r_i, p_f', P')$
        if $sign(ComputeTorqueDerivative(u, \theta, r_i, p_f', P')) > 0$ then
            $\theta \leftarrow \theta + \pi$
        end if
        $D_{new} \leftarrow UpdateScan(D', \theta)$
    until $ErrorChange(\theta) < \xi_\theta$
    return $\theta$
end function
```

By computing the axis of rotation (*ComputeAxisOfRotation*) using different methods (see section 3.4.3.A and 3.4.3.B), it is possible to perform different types of rotation.

The homogeneous transformation, T_R, is then created using the value θ just computed in the Rodrigues formula (3.62):

$$T_R = \left[\begin{array}{c|c} R(\theta) & b \\ \hline 0 & 1 \end{array}\right], \tag{3.75}$$

$$b = \begin{bmatrix} b_x \\ b_y \\ b_z \end{bmatrix} = [I - R(\theta)]\, c. \tag{3.76}$$

Note that translation b accounts for the fact that the rotation is performed with respect to center c, rather than the origin.

3.4.3.A Rotation restricted to a plane

Rotation restricted to a plane is a particular case of restricted rotations. They are performed about an axis perpendicular to the plane parallel to the image plane, and centered in the center of mass projected on this plane. Figure 3.10 shows the 3D representation of the axis and the vectors used to compute it.

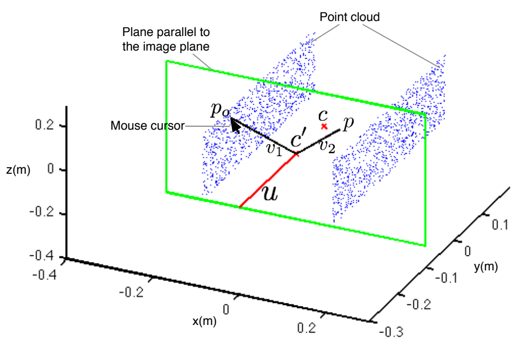

(a)

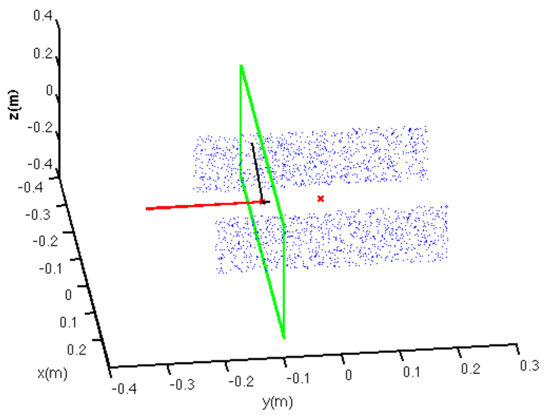

(b)

Figure 3.10: (a) 3D representation of the axis of rotation, u, orthogonal to a plane parallel to the image plane. p_o is the point cloud point clicked by the user, c' is the point cloud centroid c projected onto the plane parallel to the image plane and $v_1 \perp v_2 \perp u$. (b) 3D representation of the axis of rotation from another point of view.

The axis orthogonal to the plane, u, can be obtained by computing the cross product of two vectors belonging to the plane:

$$u = v_1 \times v_2, \tag{3.77}$$

with $v_1 = p_o - c'$ and $v_2 = p - c'$, where p_o is the the point clicked by the user, p is a point belonging to the plane, c' is the centroid project onto the plane and $v_1 \perp v_2$.

Expressions (3.71) and (3.72) are modified in order to use the centroid projected onto the plane c' instead of c, therefore $m'_k = m_k - c'$ and $d'_k = d_k - c'$.

Algorithm 3.5 shows how the axis of rotation can be computed (*ComputeAxisOfRotation*) to be used in scan adjustment algorithm 3.4.

Algorithm 3.5 Compute axis of rotation used by rotations restricted to a plane

```
function ComputeAxisOfRotation($p_o, p_f, c$)
    $c' \leftarrow ProjectCentroidOntoPlane(c)$
    $v1 \leftarrow p_o - c'$
    $v2 \leftarrow p - c'$
    $u \leftarrow v_1 \times v_2$
    return $u$
end function
```

The transformation (3.75) is created using the computed angle θ and the translation b:

$$b = \begin{bmatrix} b_x \\ b_y \\ b_z \end{bmatrix} = [I - R(\theta)]\ c', \tag{3.78}$$

where b accounts for the fact that the rotation is performed with respect to center c', rather than c.

3.4.3.B Rotation using a virtual sphere

Rotation using a virtual sphere is another particular restricted rotation. The main difference between this rotation and the rotation restricted to a plane is that, in this case, a new axis of rotation is computed everytime a drag is performed. When the user clicks on a point of the point cloud, this point is projected onto the image plane. Each time the mouse moves, the rotation axis is computed by doing the cross product between vectors v_1 and v_2 (Fig. 3.11):

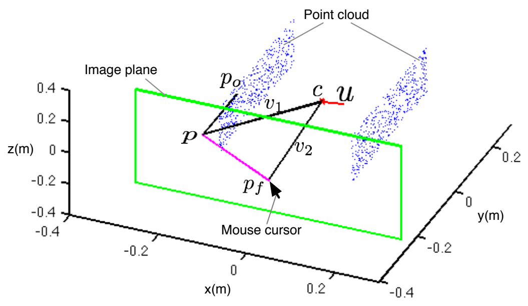

(a)

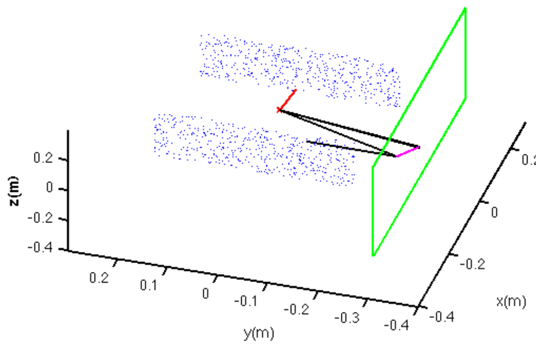

(b)

Figure 3.11: (a) 3D representation of the axis rotation, u, computed with the point p_o projected onto the image plane and the current mouse position in the image plane. p is the point clicked by the user projected onto the image plane, p_f is the mouse current position in the image plane v_1 and v_2 are vectors defined by the point cloud centroid c and p and p_f respectively. (b) 3D representation of the axis rotation from another point of view.

$$u = v_1 \times v_2, \tag{3.79}$$

with $v_1 = p - c$ and $v_2 = p_f - c$, where p is the point p_o projected onto the image plane, p_f is the mouse current position in the image plane and c is the point cloud center of mass. Although the image plane is being used to create the mouse force, note that $p_o, p_f \in R^3$. The movement of the point cloud will have a similar behaviour to a virtual sphere (see [23] for more information).

To compute the angle of rotation θ and the total torque derivative, equations (3.71) and (3.72) are used with $r_i = p - c$. Algorithm 3.6 shows the needed steps to compute the axis of rotation (*ComputeAxisOfRotation*), whenever a mouse drag is perform, for use in algorithm 3.4.

Algorithm 3.6 Compute axis of rotation used by rotations restricted to a virtual sphere

```
function ComputeAxisOfRotation($p_o, p_f, c$)
    $p \leftarrow$ project the point $p_o$ onto the image plane
    $v1 \leftarrow p - c$
    $v2 \leftarrow p_f - c$
    $u \leftarrow v_1 \times v_2$
    return $u$
end function
```

4 Results

Contents

This chapter presents the results obtained. First, a small study about the importance of defining the threshold that defines the potential field is done. Then, two user studies (one for each dimensional space) are conducted to evaluate the effectiveness, advantages and disadvantages of using each interactive mode (translations and rotations) together with the interactive alignment.

4.1 Interactive Alignment Potential Field Threshold

As said in section 3.2.2, the reaction force is produced by potential field, which is defined by a threshold ξ_{pot}. Any scan (D) that enters in this field, is automatically attracted towards the other scan (M). This effect together with the mouse force helps the user in the alignment process, by restricting the movement of the scan.

Depending on the value chosen for the threshold, the system will behave differently, helping or not the users in the alignment process. To test the influence of the threshold value on the potential field, two pairs of misaligned scans were used: one exemplifying a corridor,Fig. 4.1(a), and the other with a comb form, Fig. 4.1(b). The red part of the scans represents the common area between them (two scans are considered aligned when both red parts are overlapping). The experiment consisted in applying translations to scan D, and computing the potential function value of expression (3.9), using two different threshold values:

1. $\xi_{pot} = 0.2m$, representing a small potential field;
2. $\xi_{pot} = 30m$, representing a large potential field.

In the case of the corridor, there are three local minima solutions. As shown in Fig. 4.1(c), once scan D is near one of these minima, the movement alongside axis "y" is favoured (low potential function value) and is disfavoured alongside axis "x" (High potential function value). In this particular example, the correct alignment solution is found near the central local minima, so, as soon as the user clicks on scan, D is attracted to M by moving right. Then the user just needs to drag it a bit downwards, to correctly align them.

In the case of the scans with a comb form, Fig. 4.1(d), there are five local minima solutions. In this particular example, the correct alignment is in one of the local minima. Each local minima have a oval form, which means that when scan D is near one of them, it is automatically attracted to it. To align the scans correctly, the user just needs to perform a simple translation (with low force) in direction to the correct location.

Unlike the two previous examples, in both cases, as shown in Fig. 4.1(e) and 4.1(f), when using a high threshold value, the reaction force will make the scan D converge into the solution where both scans match perfectly, which is not the correct alignment. Moreover if the user clicks on scan D and drag it to the correct alignment location, and for some reason, he needs to interact with it a second time, the scan will move into an incorrect location, making the interactive alignment really hard to use.

The objective of the system is to make one of the scans attract to the other one when they are near to each other, and then adjust them correctly by applying mouse forces while being attracted.

For this to be possible, a small threshold value must be used. Although the value may depend on the environment structure, in all results obtained in this thesis a threshold of $0.2m$ was empirically found good enough for the system to perform well.

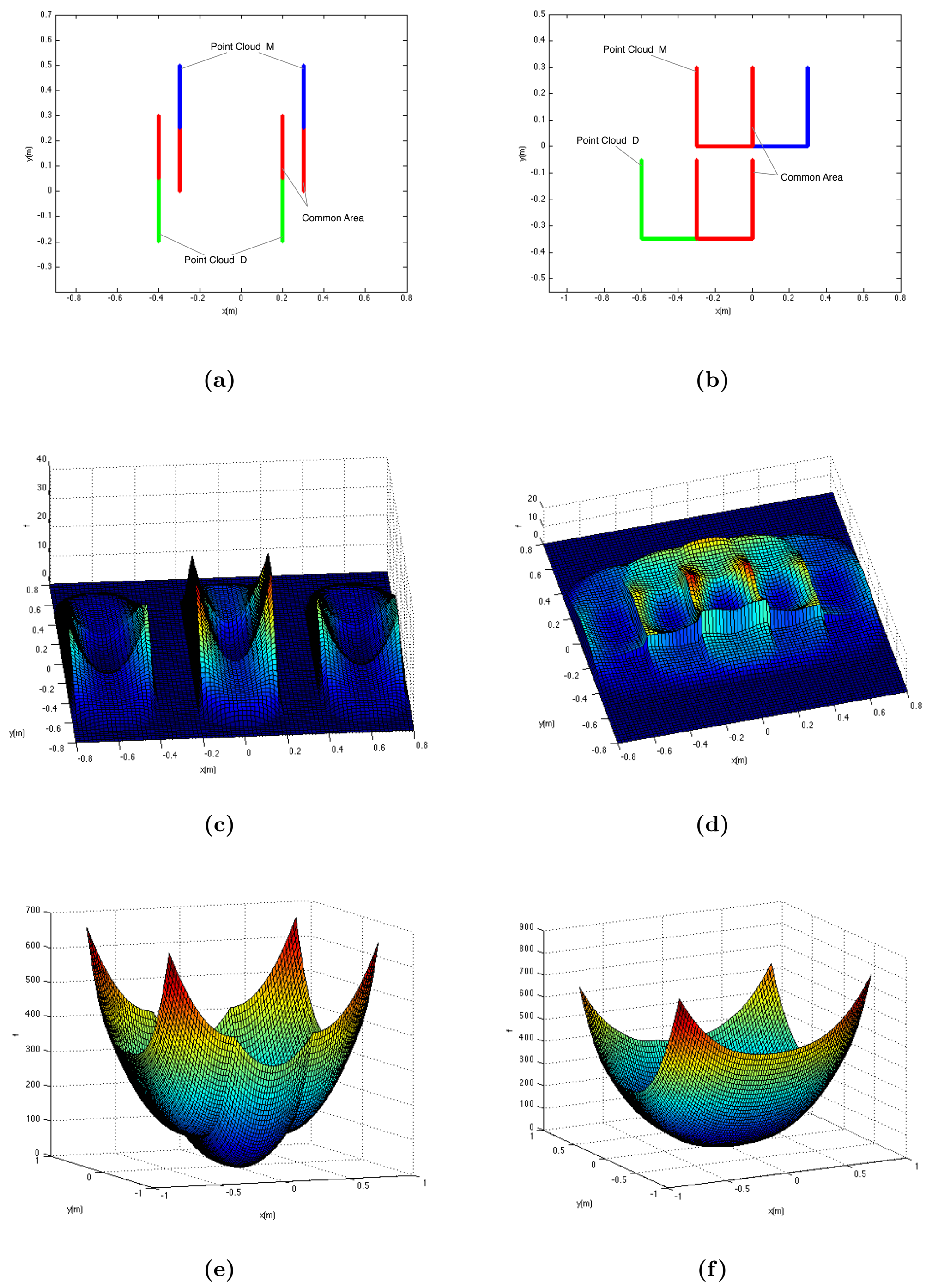

Figure 4.1: (a) Pair of scans exemplifying a corridor. (b) Pair of frames with comb form. (c) and (d) is the plot of the Reaction Potential function value when translations are performed, and using a potential field threshold of $0.2m$ (small potential field). (e) and (f) is the plot of the Reaction Potential function value when translations are performed, and using a potential field threshold of $30m$ (large potential field).

4.2 User Study for 2D alignment

A dataset was obtained with a Nomadic Scout robot with a Hokuyo LIDAR onboard. Fig. 4.2(a) shows the map of the 6th floor (ISR) of north tower of Instituto Superior Técnico (IST), where the dataset was taken from. Each scan was associated with a robot location estimated by the robot. This estimation was performed using a simple implementation of EKF together with scan matching using the LIDAR. A partial vector map of the environment was used. As a consequence, the localization algorithm got lost upon entering an office outside of its map, as shown in the upper part of Fig. 4.2(b).

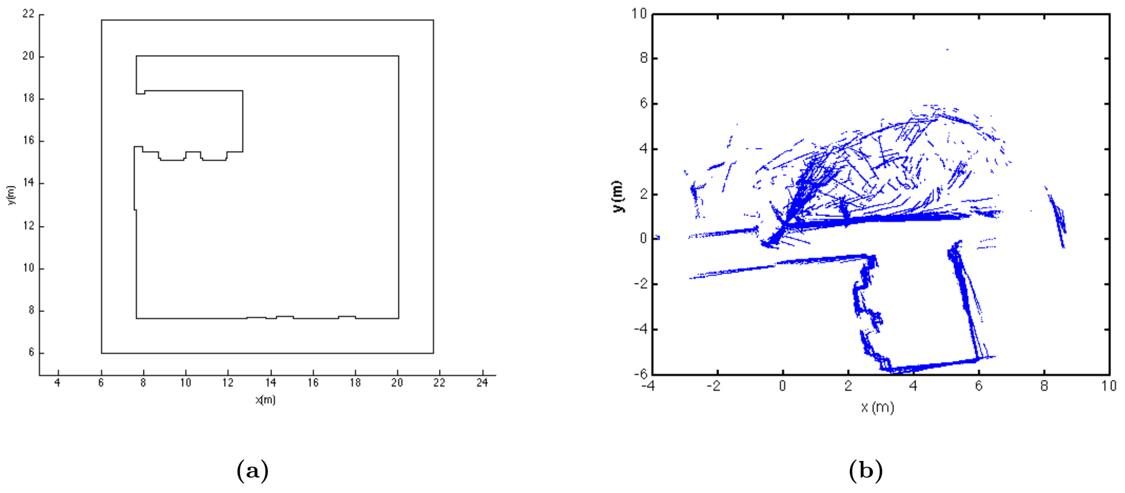

Figure 4.2: (a) Map of the sixth floor (ISR) of the north tower of IST, used to get the initial dataset. (b) Initial dataset of a map with 118 scans, obtained using a simple implementation of EKF together with scan matching using the LIDAR onboard of a Nomadic Scout robot.

In order to see how well the ICP algorithm performs, Fig. 4.3 shows four maps obtained after running it over the dataset of Fig. 4.2(b), using four different threshold values for maximum distance of closest points, $\xi_{CP} \in \{0.2\text{m}, 0.4\text{m}, 0.6\text{m}, 0.8\text{m}\}$. In general the ICP algorithm was able to align most scans, however some of them converged to a incorrect local minimum, resulting into a wrong alignment. The map obtained using a threshold $\xi_{CP} = 0.4\text{m}$, compared with the other three, appears to have more scans aligned. On the contrary, for low threshold values ($< 0.4\text{m}$), the algorithm is not able to get enough pairs of correspondences points, which results in failing to align most scans, and for high threshold values ($> 0.4\text{m}$), the algorithm obtains many pairs of points with outliers (points that do not match together), which introduces errors in the alignment.

To correct the wrong alignment and validate the proposed method, a user study was conducted by taking 8 users (75% male and 25% female with ages between 24 and 30) selected among the Master Science (MSc) students from IST. They were asked to correct the alignment of 118 frames, from a map, in two trials: with and without the use of forces. Users had no prior knowledge of the map, and everyone performed the correction of the alignment on the same initial dataset, Fig. 4.2(b).

The user performance was measured by (i) the time they took to finish the task, and by (ii) the value of the cost function, that measures how good the corrections were made. This cost function is

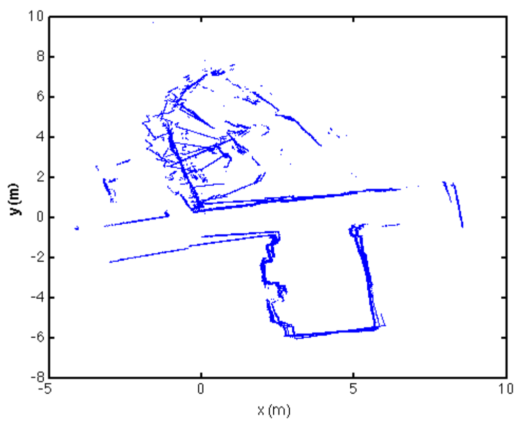

(a) $\xi_{CP} = 0.2m$

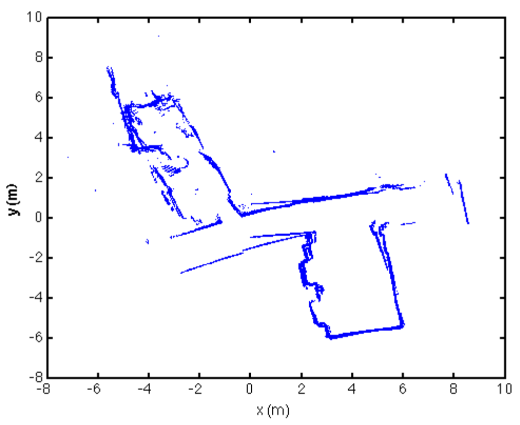

(b) $\xi_{CP} = 0.4m$

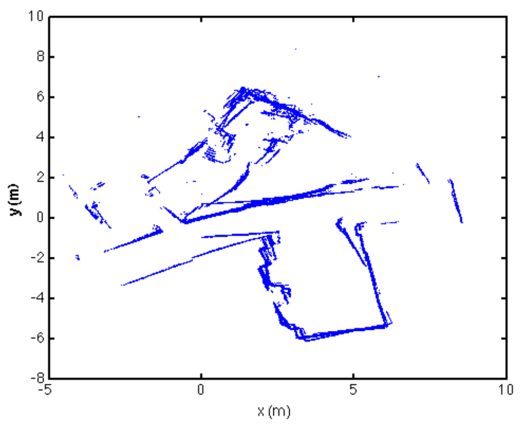

(c) $\xi_{CP} = 0.6m$

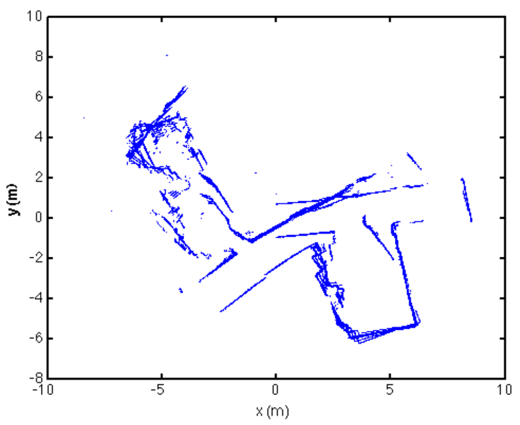

(d) $\xi_{CP} = 0.8m$

Figure 4.3: Map obtained aligning the 118 frames of the initial dataset with ICP, using different thresholds for closest points (ξ_{CP}).

the sum of the cost function for all the scan pairs:

$$f = \sum_{i=1}^{n-1} J_i, \tag{4.1}$$

where n is the number of scans and J_i is the cost function between two scans S_i and S_{i+1}, computed from expression (3.9).

If the mouse force is much higher than the reaction force, users will not feel the system restraining the movement of the scan, and consequently they will have total control over the scans. On the contrary if the reaction force is very high, the system will restrain the movement of the scans so strongly that users will not be able to move the scans as they desire. So, in order to have a good trade-off between control over the scans and help from the system, the forces proportionality constants (k_m and k_r) were empirically adjusted, so that the reaction force was slightly higher than the mouse force. In the following experiments, these values were used:

1. $k_m = 0.2$ and $k_r = 0.002$ when performing translations;

2. $k_m = 0.1$ and $k_r = 0.007$ when performing rotations;

together with a closest point threshold of 0.2 meters (note that this threshold defines the potential field).

The GUI used by the user is shown in Fig. 4.4. Information about the interface can be found in Appendix A.

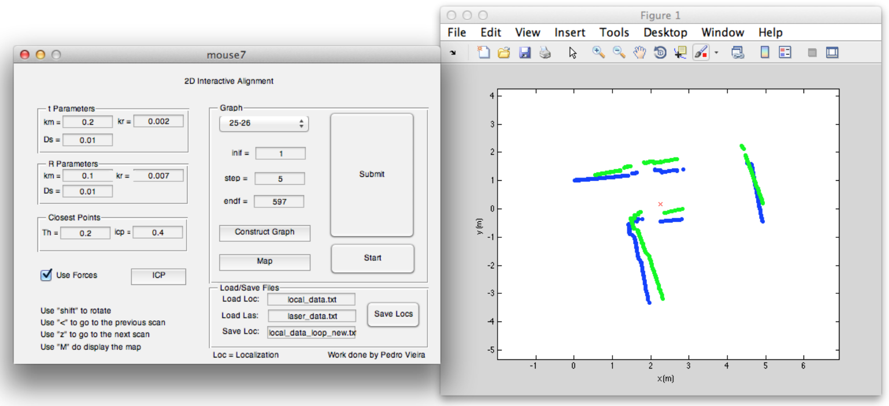
mouse7

2D Interactive Alignment

t Parameters
km = 0.2 kr = 0.002
Ds = 0.01

R Parameters
km = 0.1 kr = 0.007
Ds = 0.01

Closest Points
Th = 0.2 icp = 0.4

[✓] Use Forces ICP

Use "shift" to rotate
Use "<" to go to the previous scan
Use "z" to go to the next scan
Use "M" do display the map

Graph
25-26
inif = 1
step = 5
endf = 597

Load/Save Files
Load Loc: local_data.txt
Load Las: laser_data.txt
Save Loc: local_data_loop_new.tx

Loc = Localization Work done by Pedro Vieira

Figure 4.4: GUI implemented in Matlab and used by the user to interact with scans

After performing each one of the trials, users obtain knowledge about the initial alignment of each frame which will influence the second experiment, so to mitigate this bias, the order users do each experience is alternated between them. Half of them were asked to perform the trial without using forces first, while the other half performed the other one first. Fig. 4.5 shows an example of a map after the interactive alignment for a random user, and Fig. 4.6 shows the results obtained for each one of them.

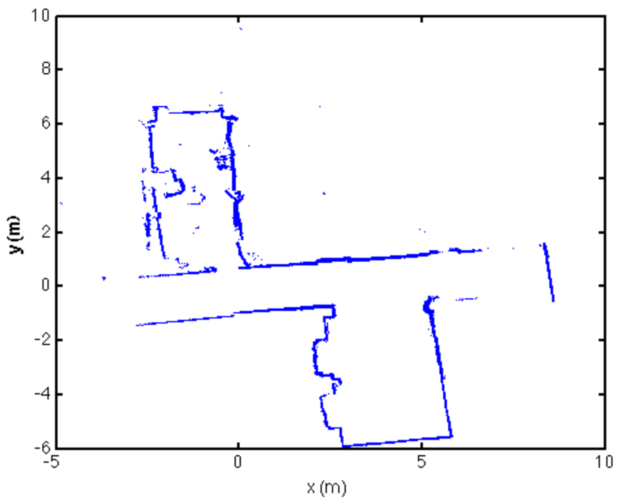

Figure 4.5: One of the maps obtained by a user after using the GUI to manually align the scans (compare with Fig. 4.2(b)).

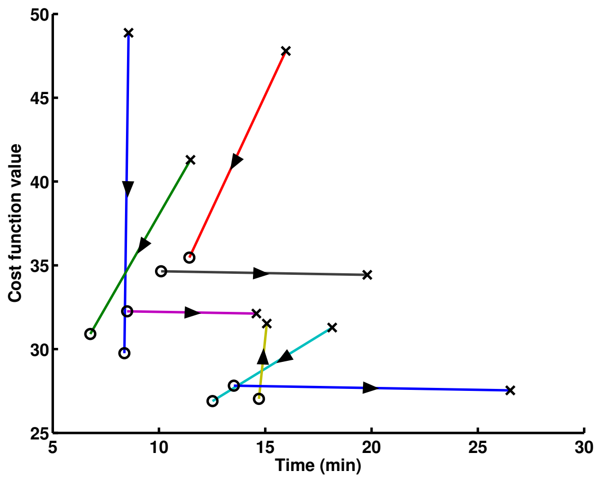

Figure 4.6: Results in terms of task completion time and cost function value obtained for each user. Each line corresponds to a user, and the "O" and the "X" markers are the results of using or not using forces. The black arrows indicate the order each user did the trials.

To analyse the effect of the forces over the time for task completion and on alignment cost value, the repeated measures analysis of variance (ANOVA) was performed on the results, using the SPSS statistics tool (version 20) from IBM. ANOVA tests the null hypotheses:

$$\mu_t^{WF} = \mu_t^F$$
$$\mu_c^{WF} = \mu_c^F$$

where μ_t^F and μ_t^{WF} are the means of the time, and μ_c^{WF} and μ_c^F are the means of the cost value, of both tasks: with (F) and without (WF) using forces. If the null hypotheses are rejected then the effect of the forces on the measures is confirmed.

The first test performed by ANOVA checks if the assumption of sphericity is met. Sphericity refers to the condition where the variances of the differences between all possible pairs of groups (i.e., levels of the independent variable) are equal. In this user study, the group representing the independent variable (trial type) only has two levels (without and using forces). For this particular type of groups (with only two levels), the sphericity assumption is always met[1].

In order to check if the use of forces have influence over the time for task completion and on cost value, ANOVA performs the test for within-subjects main effect of trial type. A factor is statistically significant if its significance value (*Sig.*) is below 0.05. The results of the test, presented in table 4.1, confirms that the use of forces strongly influences the time for task completion ($F(1,7) = 13.139$, $p < 0.05$) and the cost value ($F(1,7) = 6.249$, $p < 0.05$), but it does not say how much. Note that if the assumption of sphericity was violated the ANOVA tests would need to be corrected in order to produce more accurate significant (p) value[2].

The Partial Eta Squared, shown in table 4.1, says that 65.2% and 47.2% of the data of time and cost value respectively, is explained via this analysis of variance.

To compare the two trials and see the effect of the forces, table 4.2 shows the means and standard deviations of time and cost value for each trial. It is possible to verify that users were, in average, able to correct the alignment faster and better using forces than not using them.

Table 4.1: Test of within-subjects effects (Factor is significant if sig.<0.05)

Factor	Measure	df	df$_{error}$	F	Sig.	Partial Eta Squared
Trial Type	Time	1	7	13.139	0.008	0.652
	Cost	1	7	6.249	0.041	0.472

Table 4.2: Estimated marginal means and standard deviation values for time and cost function

Measure	Trial Type	Mean	Std. Deviation	Std. Error
Time (min)	Without F.	16.269	5.449	1.927
	With F.	10.739	2.774	0.981
Cost Value	Without F.	36.858	8.090	2.860
	With F.	30.596	3.332	1.718

At the end of the trials, users were asked to answer a questionnaire, using the well-known Likert scale as a rating criterion (from 1 to 5). The Likert statements were:

1. *The interface used for the interactive mapping was easy to use;*
2. *The use of forces makes the alignment faster;*
3. *The use of forces makes the alignment easy.*

Fig. 4.7 shows the box plot responses given by the users to each statement of the questionnaire. Overall, users responded positively to the usage of the GUI, in line with the goal of providing a system to facilitate manual alignment of range scans.

[1]See http://psychologicalstatistics.blogspot.pt/2006/05/ (retrieved 10-Oct-2012) for more details.

[2]See https://statistics.laerd.com/spss-tutorials/one-way-anova-repeated-measures-using-spss-statistics.php (retrieved 10-Oct-2012) for a review about the ANOVA steps.

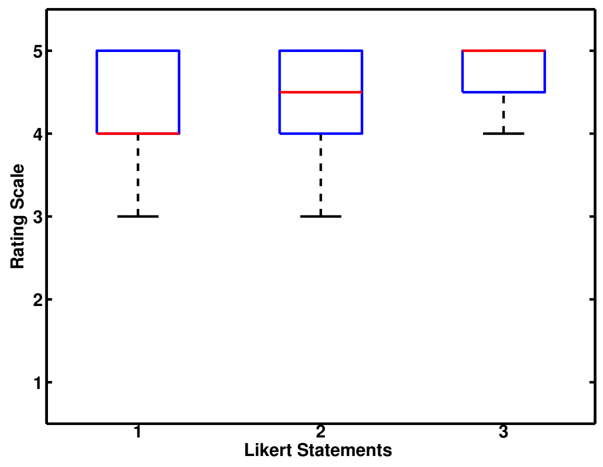

Figure 4.7: Box plot of the responses to the questionnaire. In the box plot is represented the smallest observation (in black), lower quartile (in blue), median (in red), upper quartile (in blue) and largest observation (in back).

4.3 User Study for 3D alignment

In order to evaluate the proposed method effectiveness in the 3D space, a dataset was initially obtained with a Microsoft Kinect sensor moved by hand of user over a small area inside a room, Fig. 4.8(a). While the dataset was being taken, each current scan was matched with the last scan obtained using the ICP algorithm together with the vision based algorithm presented in section 2.3. Due to the fast movement of the camera or lack of features between two consecutive frames, some pairs of scans come with errors in their alignment, Fig. 4.8(b).

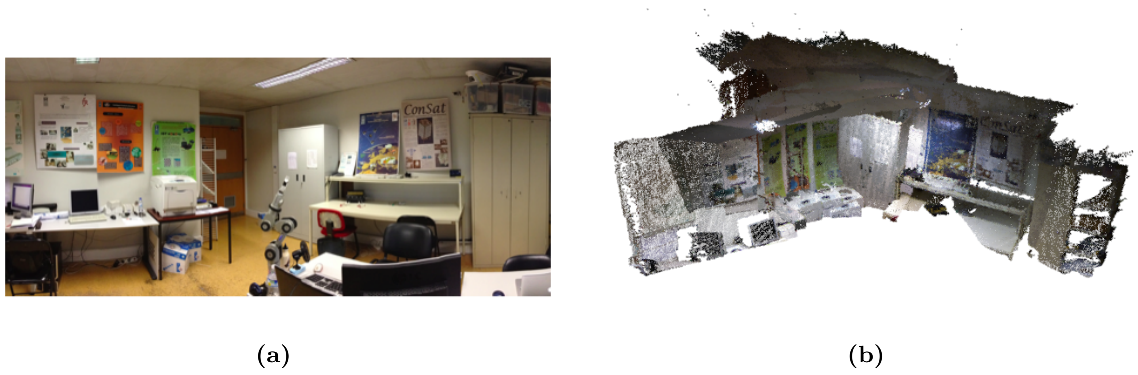

Figure 4.8: (a) Image of the area of the room used to take the dataset. (b) Initial dataset of a map with 15 scans, obtained with Microsof Kinect sensor.

To correct the misalignment and validate the proposed method in the 3D space, a user study was conducted with 12 users, most of them MSc students from IST. They were asked to correct the alignment of 15 frames, from a small area of a room, in two trials: with and without the use of forces. In order to evaluate the users performance using different rotation modes, the two trials were conducted in two experiments:

1. Aligning the 15 frames using translations and only unrestricted rotations (see section 3.4.2);

2. Aligning the 15 frames using translations and only restricted rotations (see section 3.4.3.A).

Note that there are three rotations modes presented in section 3.4, however due to the lack of time, only two of them were selected to be used in user study. The unrestricted rotation was selected because it takes into account the three DoF. From the two restricted rotations available, the one restricted to a plane was selected for being more easy and intuitive to use.

Users had no prior knowledge of the initial alignment of each pair of scans, and everyone performed their correction on the same initial dataset (Fig. 4.8(b)).

The user performance was measure in the same way as in section 4.2, by (i) the time they took to finish the task, and by (ii) the value of the cost function, that measures how good the corrections were made. Expression (4.1) was used to compute the value of the cost function.

The forces proportional constants (k_m and k_r) were empirically adjusted in the same way as in section 4.2, and the following values were used:

1. $k_m = 0.2$ and $k_r = 0.005$ when performing translations;

2. $k_m = 0.1$ and $k_r = 0.001$ when performing rotations;

together with a closest point threshold of 0.2 meters. The GUI used in the experiments is explained in detail in Appendix B.

Before starting each experiment, users had 5 minutes of explanation about the interface usage and in order to familiarize themselves with the rotation mode being used, they had more 5 minutes of training with it, in order to mitigate any bias caused by the learning curve effect.

After doing one of the experiments, users obtain knowledge about the initial alignment of each frame and get used to the interface, which will influence the remaining experiments. So to mitigate this bias, half of them were asked to do the experiment using unrestricted rotation first, while the other half were asked to use restricted rotations first. In each experiment, 3 of the 6 users were asked to perform the trial without using forces first, while the other 3 were asked to perform the trial with forces first. Fig. 4.9 shows an example of a map after the interactive alignment for a random user, and Fig. 4.10 shows the results obtained for each one of them in each experiment (for more details see Appendix C).

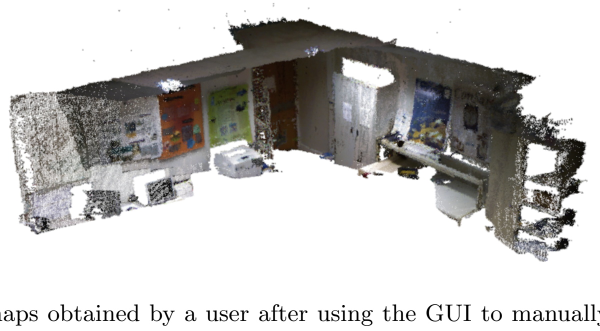

Figure 4.9: One of the maps obtained by a user after using the GUI to manually align the scans (compare with Fig. 4.8).

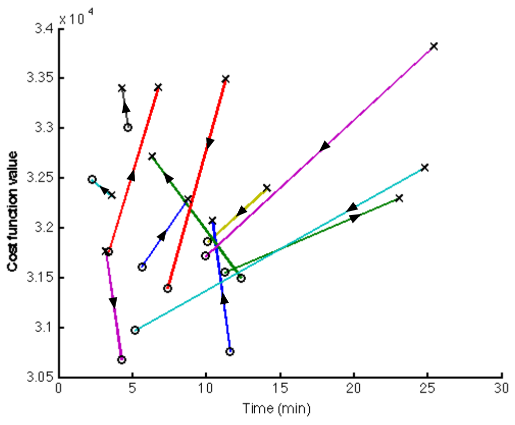

(a) Results using unrestricted rotations

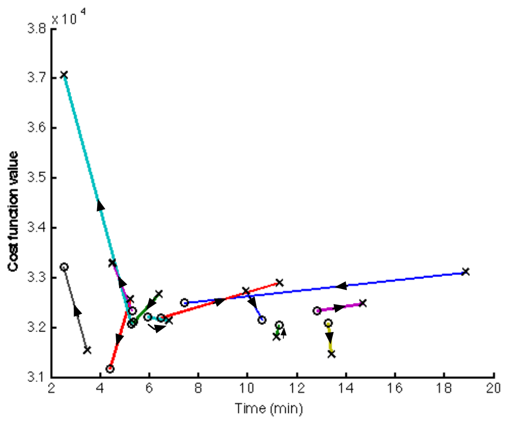

(b) Results using restricted rotations

Figure 4.10: Results in terms of task completion time and cost function value obtained for each user and experiment. Each line corresponds to a user, and the "O" and the "X" markers are the results of using or not using forces respectively. The black arrows indicate the order each user did the trials.

To analyse the effect of the forces and rotations on the time of task completion and on alignment cost value, the ANOVA test was also performed on the results, like in section 4.2, but in this case using two groups (factors) each with two levels:

1. Rotation Type: Unrestricted and Restricted;
2. Trial Type: Without Forces and with Forces.

In this case, ANOVA tests the null hypotheses for the two factors in separately and for the interaction between them. As in section 4.2, the assumption of sphericity is met, for this type of groups. Table 4.3 shows the results of the test within-subjects of both measures (time and cost value). As it can be seen, the significant p-values (*Sig.*) show that the use of forces have an effect on the time ($F(1, 11) = 5.97$, $p < 0.05$) and on the cost value ($F(1, 11) = 14.45$, $p < 0.05$), however the type of rotation and the interaction between forces and rotations did not came out statistical significant on both time and cost value ($p > 0.05$), which means that users have almost the same performance using either rotation type and the effect of the use of forces is not substantial when using either rotation.

The Partial Eta Squared, from table 4.3, says and confirms that the effect size of rotation type and the interaction between rotations and trials on both measures was very small. However, for the trial type factor, 35.2% and 56.8% of the data of time and cost value were explained with this analysis of variance.

Table 4.3: Test of within-subjects effects (Factor is significant if sig.<0.05)

Factor	Measure	df	df$_{error}$	F	Sig.	Partial Eta Squared
Trial Type	Time (min)	1	11	5.97	0.033	0.352
	Cost	1	11	14.45	0.003	0.568
Rotation Type	Time (min)	1	11	1.38	0.265	0.111
	Cost	1	11	1.74	0.215	0.136
Trial Type × Rotation Type	Time (min)	1	11	1.66	0.224	0.131
	Cost	1	11	0.80	0.390	0.068

Table 4.4: Estimated marginal means of time and cost value considering only the trial type

Measure	Trial Type	Mean	Std. Error
Time (min)	Without Forces	10.407	1.665
	With Forces	7.424	0.938
Cost Value	Without Forces	3.277×10^4	2.087×10^2
	With Forces	3.191×10^4	1.330×10^2

Table 4.5: Estimated marginal means of time and cost value considering only the rotation type

Measure	Rotation Type	Mean	Std. Error
Time (min)	Unrestricted	9.561	1.485
	Restricted	8.270	1.143
Cost Value	Unrestricted	3.216×10^4	1.618×10^2
	Restricted	3.251×10^4	2.106×10^2

Table 4.6: Estimated marginal means and standard deviation values of time and cost value for the interaction between rotation and trial

Trial Type	Measure	Rotation Type	Mean	Std. Deviation	Std. Error
Without Forces	Time (min)	Unrestricted	11.809	8.259	2.384
		Restricted	9.004	5.035	1.454
	Cost Value	Unrestricted	3.272×10^4	6.548×10^2	1.890×10^2
		Restricted	3.282×10^4	14.628×10^2	4.222×10^2
With Forces	Time (min)	Unrestricted	7.313	3.548	1.024
		Restricted	7.536	3.542	1.023
	Cost Value	Unrestricted	3.161×10^4	6.665×10^2	1.924×10^2
		Restricted	3.221×10^4	4.566×10^2	1.318×10^2

Table 4.4, 4.5 and 4.6 show the means and standard deviations of the time and the cost value for each trial considering only the trial type, only the rotation type and the interaction between them respectively. The first table shows that users were able to correct the alignment faster and more accurately. Since the rotation type and the interaction between rotations and trials are not significance, it is not possible to draw conclusions from the other two tables.

At end of the experiments, users were asked to answer a questionnaire. In 5 of the questions, they used the Likert scale as a rating criterion (from 1 to 5). The Likert statements were:

1. *The use of forces made the alignment easy*
2. *The use of forces makes the alignment easy*
3. *With forces, unrestricted rotations are preferable over the restricted one*
4. *Without forces, restricted rotations are easier to control*
5. *The interface used for the interactive mapping was easy to use*

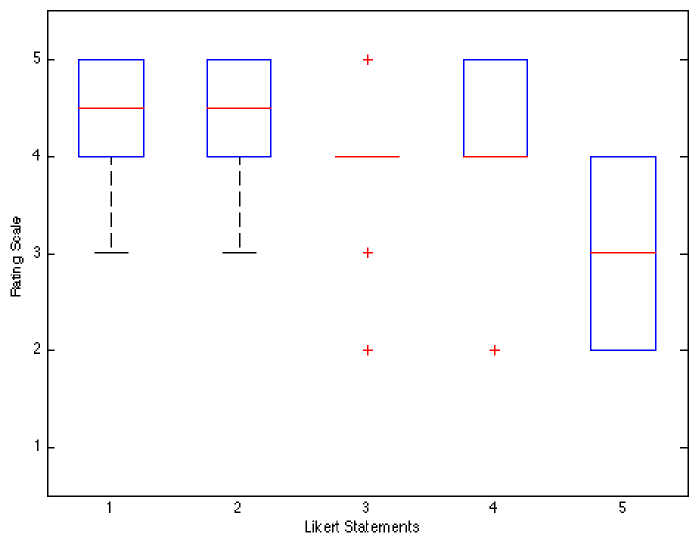

Figure 4.11: Box plot of the responses to the questionnaire. In the box plot is represented the smallest observation (in black), lower quartile (in blue), median (in red), upper quartile (in blue) and largest observation (in back). The "+" symbols correspond only to one answer.

Fig. 4.11 shows the box plot responses given by the users to each statements of the questionnaire. Some of the users did not respond positively and most of them were indifferent to the use of the interface. Users claimed that the way of rotating the camera view was hard and not intuitive. They also said that sometimes they did not know which points belonged to each scan. Overall, users responded positively to the use of forces in the alignment and agree that restricted rotations are easier to control without forces, and unrestricted rotations are preferable when using forces.

The following questions were also asked to the users:

1. *Do you have experience working with interfaces for interacting with objects (e.g. by applying translations and rotations)? (Yes, Some, No)*
2. *During the experiments with forces, was there any time you wished switch off the forces? (Yes, No)*
3. *Using forces, if you had to chose one rotation mode to interact with scans, what would it be? (Unrestricted rotation, restricted rotation)*
4. *Without using forces, if you had to chose one rotation mode to interact with scans, what would it be? (Unrestricted rotation, restricted rotation)*

Fig. 4.12 shows the results of the answers given to the questions in percentage. Most of the users that participated in the user study had little or almost no experience with interfaces used to interact with 3D objects. This made the users spend more time getting used to interface controllers in the beginning of the first experience. More than half of them wished to turn off the forces when they were aligning some pairs. Finally most of the users preferred using unrestricted rotations together with force, and only 1 preferred to use the unrestricted rotation mode to interact with point clouds when forces are switch off.

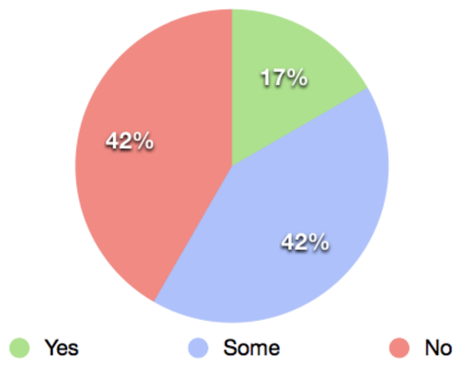

(a) Do you have experience working with interfaces for interacting with objects (by applying translations and rotations)?

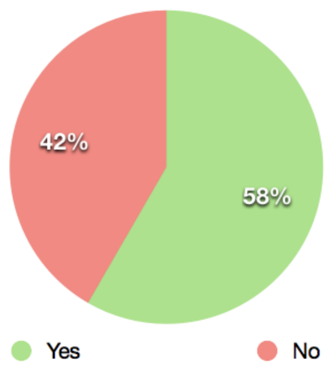

(b) During the experiments with forces, was there any time you wished turn off the forces?

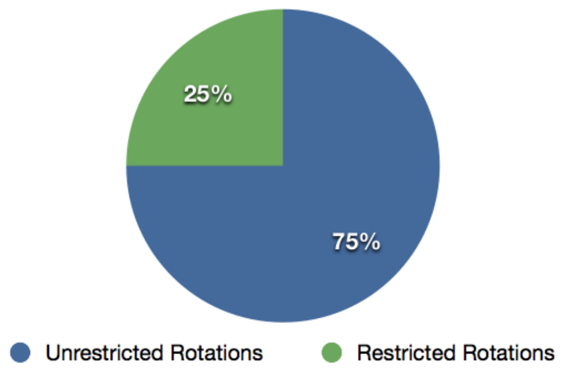

(c) Using forces, if you had to chose one rotation mode to interact with scans, what would it be?

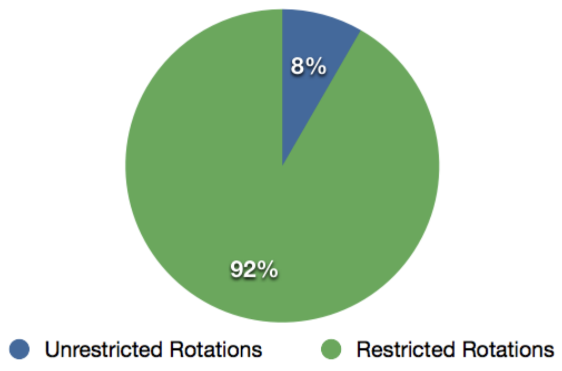

(d) Without using forces, if you had to chose one rotation mode to interact with scans, what would it be?

Figure 4.12: Charts with the users responses of the questionnaire in percentage.

5 Conclusion

Contents

In this chapter, this thesis ends with some conclusions, and draws some future directions in this field of research.

5.1 Conclusion

This thesis proposed a method which uses virtual forces with the purpose of aiding users to manually adjust the alignment of RGB-D point clouds. The method works in a system where users manually align pairs of point clouds, using a GUI and a computer mouse, by applying either translations or rotations to one of them. The method helps the users in the alignment process by restraining the movement of the point clouds. Scans are aligned by balancing a force produced by a mouse drag with a reaction force produced by a potential field.

In order to help the users in the matching process, the threshold which defines the potential field (ξ_{pot}) had to be carefully adjusted. The method restrains the movement of point clouds by attracting them to the nearest local minima. If the value of the threshold is too small the reaction force will be low, making the attraction effect insignificant. On the contrary if the value is too high the reaction force will be very strong, making point clouds to converge to a global minima and consequently making the alignment quite irritating for users.

To validate the proposed method in both 2D and 3D spaces, two user studies were conducted, where users were asked to preform the task of correcting the alignment of a set of point clouds, with and without the use of forces. The time of task completeness and the cost value that measures how well two scans are aligned were measured to evaluate the users performance. The results of both user studies were analysed on both measures (time and cost) using the ANOVA test, which suggested that the use of forces had a significant effect on the measures and showed that users performed better using forces than not using them. In the 3D user study, users performed each task (with and without using forces) using two different rotation modes. The results of the ANOVA test suggested that the effect of type of rotation and the interaction between rotation and task type on the measures were not statistically significant. Overall, users were able to obtain a more accurate map and align all pairs of point clouds faster with the use of forces.

In the end of each user study, users gave their opinion by answering a simple questionnaire. In general they found the proposed method to be a valuable aid in the correction of the alignment, making it faster and more easy to use, specially in the 3D space, where the interaction with point clouds, using a computer mouse, is hard. Users also found the interaction with the interface not easy to use. They had specially a hard time to get used to the rotation controller of the camera viewer, saying that it was not intuitive. Between the two rotations modes used in the 3D user study (unrestricted and restricted rotations), users preferred the restricted rotation when forces were switched off, due to the two DoF, since they were much easier to control. On the other hand. when using forces, users reported that unrestricted rotations behaved better than the restricted one, and they needed less actions with the camera viewer to align the scans.

5.2 Future Work

The proposed method was tested on datasets with very structured environments, like rooms and corridors. Users are particularly familiar and used to this kind of environments, making it easy for them to find out how certain scans match together. It would be interesting to conduct some tests, with users, in a more complex and unstructured scenarios, like the ones usually used in SaR missions, and see how they perform.

During the realization of the 3D user study some issues regarding the interface were found:

1. The rotation method used to rotate the camera viewer was hard to use.
2. Users had hard time to distinguish the two scans being align, which made them sometimes mess up the alignment just to find out which scan was which.
3. Due to the low resolution of some pairs of frames, users felt difficulties in recognizing same patterns in these frames.
4. Users complained in the usage of some keys of the keyboard.

These issues must be resolved in a future version of the interface. The actions of the keys should be conceived in a more user friendly way, and some useful actions, like the capacity of doing undo to the alignment performed, should be include into the interface. Users should also be able to switch on and off the use of forces when they desire, since in some cases they may not help them.

The type of graph used in this thesis to organise scans and build the map was rather limited. Also, the maps were built using always all points available in the point clouds, which makes it computationally expensive when presenting the maps to the users in the interface. A more efficient way of maintaining the map in memory should be think of.

One promising application would be to use the proposed method in a semi-automatic system, where it prompts the user when is unsure about the alignment of two point clouds. At this point, the user "helps" the system.

It could be interesting to extend the proposed method to the alignment of multiple scans, instead of only two at a time, for instance to approach the problem of loop closures. In this kind of problem, we already have a map with a certain shape, thus by trying to perform a loop closure on it, users would need to interact with multiple scans at the same time, in order to have global view of the map.

Finally the method could also be used together with the ICP algorithm. Since ICP some times converge to an incorrect local minima, the interactive alignment could be useful to take point clouds from that minima, and placing them near the right solution, and then run again ICP to automatically align the scans. It would be interesting to see how users perform in the alignment process when using both ICP and interactive alignment.

Bibliography

[1] D. A. Simon, "Fast and accurate shape-based registration," Ph.D. dissertation, Carnegie Mellon University, Pittsburgh, PA, USA, 1996.

[2] S.-Y. Park, J. Baek, and J. Moon, "Hand-held 3D scanning based on coarse and fine registration of multiple range images," *Machine Vision and Applications*, vol. 22, no. 3, pp. 563–579, May 2011.

[3] P. Biber, H. Andreasson, T. Duckett, and A. Schilling, "3D modeling of indoor environments by a mobile robot with a laser scanner and panoraic camera," in *IEEE/RSJ International Conference on Intelligent Robots and Systems (IROS'04)*, vol. 4, Sept. 2004, pp. 3430–3435.

[4] S. Thrun, "Robotic mapping: A survey," in *Exploring Artificial Intelligence in the New Millenium.* Morgan Kaufmann, 2002, pp. 1–35.

[5] A. Elfes, "Autonomous robot vehicles," I. J. Cox and G. T. Wilfong, Eds. New York, NY, USA: Springer-Verlag New York, Inc., 1990, ch. Sonar-based real-world mapping and navigation, pp. 233–249.

[6] S. Thrun, "Learning occupancy grid maps with forward sensor model," *Autonomous Robots*, vol. 15, no. 2, pp. 111–127, 2003.

[7] F. Lu and E. Milios, "Globally consistent range scan alignment for environment mapping," *Autonomous robots*, vol. 4, no. 4, pp. 333–349, 1997.

[8] S. Thrun, W. Burgard, and D. Fox, "A real-time algorithm for mobile robot mapping with applications to multi-robot and 3D mapping," in *IEEE International Conference on Robotics and Automation (ICRA'00)*, vol. 1, 2000, pp. 321–328.

[9] D. Murray and C. Jennings, "Stereo vision based mapping and navigation for mobile robots," in *IEEE International Conference on Robotics and Automation (ICRA'97)*, vol. 2, Apr 1997, pp. 1694–1699.

[10] S. N. Sinha, D. Steedly, R. Szeliski, M. Agrawala, and M. Pollefeys, "Interactive 3D architectural modeling from unordered photo collections," *ACM Transactions on Graphics (TOG)*, vol. 27, no. 5, pp. 159:1–159:10, Dec. 2008.

[11] P. Henry, M. Krainin, E. Herbst, X. Ren, and D. Fox, "RGB-D mapping: Using depth cameras for dense 3D modeling of indoor environments," in *The 12th International Symposium on Experimental Robotics (ISER'10)*, 2010.

[12] K. Lai, L. Bo, X. Ren, and D. Fox, "A large-scale hierarchical multi-view RGB-D object dataset," in *IEEE International Conference on Robotics and Automation (ICRA'11)*, 2011, pp. 1817–1824.

[13] D. Borrmann, J. Elseberg, K. Lingemann, A. Nüchter, and J. Hertzberg, "Globally consistent 3D mapping with scan matching," *Robotics and Autonomous Systems*, vol. 56, no. 2, pp. 130–142, 2008.

[14] J. Gutmann and K. Konolige, "Incremental mapping of large cyclic environments," in *IEEE International Symposium on Computational Intelligence in Robotics and Automation (CIRA'99)*, 1999, pp. 318–325.

[15] P. Newman, G. Sibley, M. Smith, M. Cummins, A. Harrison, C. Mei, I. Posner, R. Shade, D. Schroeter, D. Cole, and I. Reid, "Navigating, recognising and describing urban spaces with vision and laser," *The International Journal of Robotics Research*, vol. 28, no. 11–12, pp. 1406–1433, 2009.

[16] F. Dellaert and D. Bruemmer, "Semantic SLAM for collaborative cognitive workspaces," in *AAAI Fall Symposium Series 2004: Workshop on The Interaction of Cognitive Science and Robotics: From Interfaces to Intelligence*, 2004.

[17] A. Diosi, G. Taylor, and L. Kleeman, "Interactive SLAM using laser and advanced sonar," in *IEEE International Conference on Robotics and Automation (ICRA'05)*, Apr 2005, pp. 1103–1108.

[18] H. Du, P. Henry, X. Ren, M. Cheng, D. B. Goldman, S. M. Seitz, and D. Fox, "Interactive 3D modeling of indoor environments with a consumer depth camera," in *13th International Conference on Ubiquitous Computing (UbiComp'11)*, Sept. 2011, pp. 75–84.

[19] P. Henry, M. Krainin, E. Herbst, X. Ren, and D. Fox, "RGB-D mapping: Using kinect-style depth cameras for dense 3D modelling of indoor environments," *International Journal of Robotics Research*, vol. 31, no. 5, pp. 647–663, 2012.

[20] M. A. Fischler and R. C. Bolles, "Random sample consensus: a paradigm for model fitting with applications to image analysis and automated cartography," *Communications of the ACM*, vol. 24, no. 6, pp. 381–395, Jun. 1981.

[21] P. J. Besl and N. D. McKay, "A method for registration of 3-D shapes," *IEEE Transactions on Pattern Analysis and Machine Intelligence*, vol. 14, no. 2, pp. 239–256, Feb. 1992.

[22] M. Chen, S. J. Mountford, and A. Sellen, "A study in interactive 3-D rotation using 2-D control devices," *ACM SIGGRAPH Computer Graphics*, vol. 22, no. 4, pp. 121–129, Aug. 1988.

[23] R. Bade, F. Ritter, and B. Preim, "Usability comparison of mouse-based interaction techniques for predictable 3D rotation," in *5th International Conference on Smart Graphics (SG'05)*, Aug. 2005, pp. 138–150.

[24] Y. J. Zhao, D. Shuralyov, and W. Stuerzlinger, "Comparison of multiple 3D rotation methods," in *IEEE International Conference on Virtual Environments, Human-Computer Interfaces, and Measurement Systems (VECIMS'11)*, Sept. 2011, pp. 13–17.

[25] P. Vieira and R. Ventura, "Interactive mapping in 3D using RGB-D data," in *10th IEEE International Symposium on Safety Security and Rescue Robotics (SSRR'12)*, 2012.

[26] P. Vieira and R. Ventura, "Interactive 3D scan-matching using RGB-D data," in *17th IEEE International Conference on Emerging Technologies & Factory Automation (ETFA'12)*, 2012.

[27] P. Vieira and R. Ventura, "Interactive mapping using range sensor data under localization uncertainty," in *1th International Workshop on Perception for Mobile Robots Autonomy (PEMRA'12)*, 2012.

[28] P. Vieira and R. Ventura, "Interactive mapping using range sensor data under localization uncertainty," *Journal of Automation, Mobile Robotics & Intelligent Systems (JAMRIS)*, 2012, in press.

[29] S. Rusinkiewicz and M. Levoy, "Efficient variants of the ICP algorithm," in *3th IEEE International Conference on 3-D Digital Imaging and Modeling (3DIM'01)*, 2001, pp. 145–152.

[30] T. Masuda, K. Sakaue, and N. Yokoya, "Registration and integration of multiple range images for 3-D model construction," in *13th IEEE International Conference on Pattern Recognition (ICPR'96)*, Aug. 1996, pp. 879–883.

[31] Z. Zhang, "Iterative point matching for registration of free-form curves and surfaces," *International Journal of Computer Vision*, vol. 13, no. 2, pp. 119–152, Oct. 1994.

[32] K. S. Arun, T. S. Huang, and S. D. Blostein, "Least-squares fitting of two 3-D point sets," *IEEE Transactions on Pattern Analysis and Machine Intelligence*, vol. 9, no. 5, pp. 698–700, May 1987.

[33] B. K. P. Horn, "Closed-form solution of absolute orientation using unit quaternions," *Journal of the Optical Society of America A*, vol. 4, no. 4, pp. 629–642, 1987.

[34] B. K. P. Horn, H. Hilden, and S. Negahdaripour, "Closed-form solution of absolute orientation using orthonormal matrices," *Journal of the Optical Society of America*, vol. 5, no. 7, pp. 1127–1135, 1988.

[35] M. W. Walker, L. Shao, and R. A. Volz, "Estimating 3-D location parameters using dual number quaternions," *CVGIP: Image Understanding*, vol. 54, no. 3, pp. 358–367, Nov. 1991.

[36] D. W. Eggert, A. Lorusso, and R. B. Fisher, "Estimating 3-D rigid body transformations: a comparison of four major algorithms," *Machine Vision and Applications*, vol. 9, no. 5-6, pp. 272–290, Mar. 1997.

[37] Y. Chen and G. Medioni, "Object modelling by registration of multiple range images," *Image and Vision Computing*, vol. 10, no. 3, pp. 145–155, Apr. 1992.

[38] K.-L. Low, "Linear least-squares optimization for point-to-plane ICP surface registration," Department of Computer Science, University of North Carolina at Chapel Hill, Tech. Rep. TR04-004, Feb. 2004.

[39] A. Segal, D. Haehnel, and S. Thrun, "Generalized-ICP," in *Robotics: Science and Systems*, Seattle, USA, Jun. 2009.

[40] D. G. Lowe, "Object recognition from local scale-invariant features," in *IEEE International Conference on Computer Vision (ICCV '99)*, vol. 2, 1999, pp. 1150–1157.

[41] H. Bay, A. Ess, T. Tuytelaars, and L. V. Gool, "Speeded-up robust features SURF," *Computer Vision and Image Understanding*, vol. 110, no. 3, pp. 346–359, Jun. 2008.

[42] E. Rublee, V. Rabaud, K. Konolige, and G. Bradski, "ORB: An efficient alternative to SIFT or SURF," in *IEEE International Conference on Computer Vision (ICCV'11)*, Nov. 2011.

[43] J. J. Craig, *Introduction to Robotics: Mechanics and Control*, 2nd ed. Boston, MA, USA: Addison-Wesley Longman Publishing Co., Inc., 1989.

A

2D Interface Manual

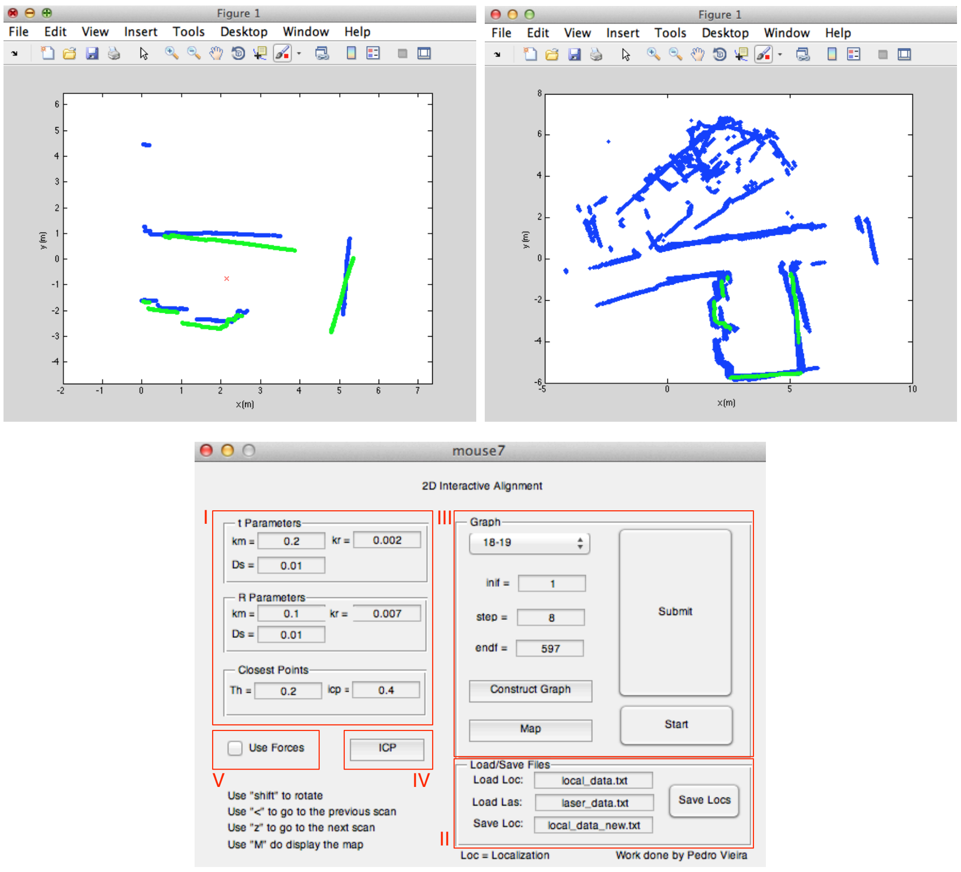

t Parameters: km = 0.2, kr = 0.002, Ds = 0.01

R Parameters: km = 0.1, kr = 0.007, Ds = 0.01

Closest Points: Th = 0.2, icp = 0.4

Use Forces

Graph: 18-19, inif = 1, step = 8, endf = 597

Load/Save Files: Load Loc: local_data.txt; Load Las: laser_data.txt; Save Loc: local_data_new.txt

Use "shift" to rotate
Use "<" to go to the previous scan
Use "z" to go to the next scan
Use "M" do display the map

Loc = Localization

Work done by Pedro Vieira

Figure A.1: Interface used for test the Interactive Alignment in the 2D space. Upper left figure shows a pair of scans being align, and the upper right shows the map and the current frame being align (map only appears when the user is pressing a designated key from the keyboard).

The interface used to interact with 2D range scans and test the Interactive Alignment, was develop in *Matlab*^{TM} *R2011a*. The interface is divided in five blocks and an external window, where the interaction between users an range scans takes place.

On **Block I** users can define all constants and thresholds of the system. For each interactive mode, users can define the forces constants (k_m and k_r) and the threshold (ξ_t and ξ_R in meters) used to check if forces are balanced. Users can also define the threshold (in meters) for closest points for both ICP algorithm ($icp \leftrightarrow \xi_{CP}$) and Interactive Alignment ($Th \leftrightarrow \xi_{pot}$).

On **Block II** users can load the file with the LIDAR data containing the scans points information, and the file with the scans respective position along time. These files are organized like shown in table A.1.

Table A.1: Structure of the Scans data and localization files

Localizations(**loc**)	$time\ x_1\ y_1\ \theta_1$ $time\ x_2\ y_2\ \theta_2$ $time\ x_n\ y_n\ \theta_n$
LIDAR data (**las**)	$time\ point_1^1\ point_1^2\ point_1^3\ ....\ point_1^N$ $time\ point_2^1\ point_2^2\ point_2^3\ ....\ point_2^N$ $time\ point_n^1\ point_n^2\ point_n^3\ ....\ point_n^N$

As soon as the users write the files names, the box "endf", from Block III, is updated with the total number of scans present in the data file. Users can at any time press the button “Save Locs” to save the current position of the scans with the same format as the one shown in table A.1.

After writing the name of the scans data and localization files, users press the button “Construct Graph”, in **Block III**, to construct the graph. The frequency of data acquisition from LIDAR is high, and many obtained scans contain redundant information, not important for users. So they can choose the initial and final scans as well as the step that the program is going to read the file. By pushing the “map” button, the map with the current alignment is displayed on the interactive window. The “start” and the “submit” buttons were used in the user study to measure the time users took to align all scans (see section 4.2). The pop-up window above the “inif” box, lets the user chose which pair of scans from the graph he wants to align.

The button in **Block IV** performs the ICP algorithm to each pair of scans in the graph.

The check box in **Block V** turns on or off the use of the reaction force in the interactive alignment system.

The interaction between the user and the interface is done using a computer mouse and a keyboard. The mouse is used to interact directly with range scans. With it, users correct the alignment of the scans by applying either translations or rotations. Translations can be performed by simply clicking on the green scan and dragging it. Slightly different, Rotations are performed by clicking on the scan and dragging it, while pressing on one designated key from the keyboard. Table A.2 shows the keys that users can use to interact with the interface.

Table A.2: Valid Keys from the keyboard accepted by the interface

Keys	Description
shift	while pressing, enables rotation mode
<	goes to the previous pairs of scans of the graph (previous edge)
z	goes to the next pair of scans of the graph (next edge)
m	while pressing, shows actual alignment of the map on the window in blue, and the current scan being align in green

B

3D Interface Manual

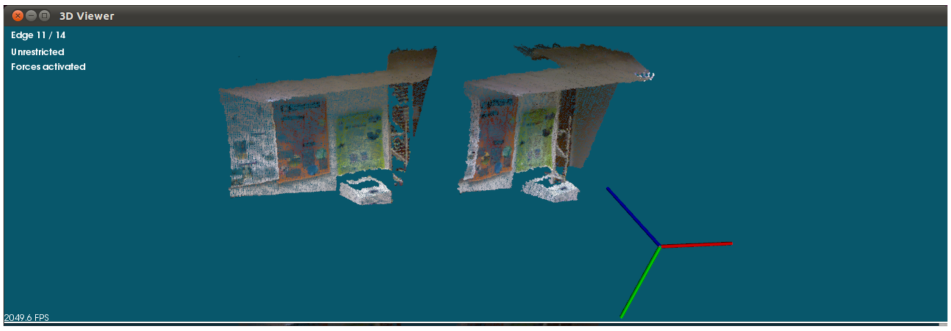

(a) Scans Viewer

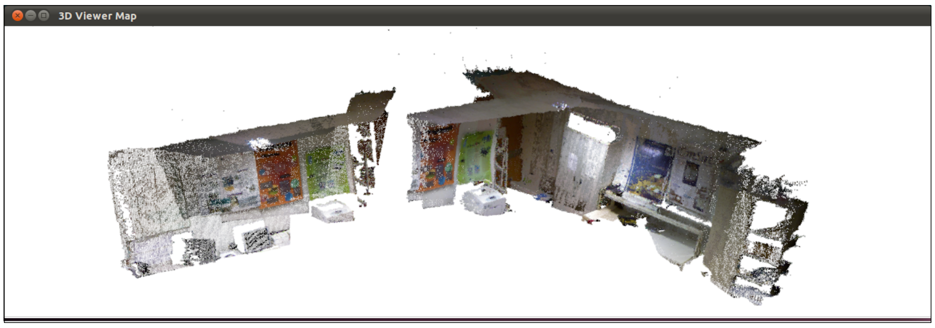

(b) Map Viewer

Figure B.1: 3D Interface used for the Interactive Alignment

The interface built to interact with scans ranges in 3D, was written in *C++* using the Point Cloud Library[1] (PCL). The interface is composed of two viewer windows (Fig. B.1):

Scans Viewer: The Interaction between users and point clouds is performed in this viewer. Point clouds are presented in pairs of two. Users can interact with both of them by applying either translations or rotations with a computer mouse. The information about the *edge of the graph* where the user is working on, the *rotation mode* being used and if the *forces* are turned on or off, is displayed in the upper left corner of the viewer.

Map Viewer: The map of the environment (stored in the graph) is displayed in this viewer. This viewer serves only for visualisation purposes, thus users cannot interact with point clouds in it.

Users interact with the interface using a computer mouse and keyboard. In table B.1 and in B.2 is a detailed description of the actions and keys users can use with a mouse and with a keyboard respectively. The keys in the table B.2 only work on the Scans Viewer. In the Map Viewer, users are only allowed to change the viewer camera position and view.

[1]http://www.pointclouds.org (retrieved 10-Oct-2012)

Table B.1: Actions of the mouse buttons

Buttons	Description
Left	Pick a point of a point cloud to interact with it (while *shift* key is being pressed)
Middle wheel	Zoom in/out
Middle wheel	While pressed, allows users to make translations to the viewer camera position
Right	Changes the viewer camera view

Table B.2: Actions of the keyboard keys

Keys	Description
shift	enables picking a point of a point cloud, to perform translations
shift+ctrl	enables picking a point of a point cloud, to perform rotations
Q	quits the interface
$<$	goes to the previous pair of point clouds of the graph (previous edge)
Z	goes to the next pair of point clouds of the graph (next edge)
1	switches on/off forces
2	changes the rotation mode (*unrestricted*, *restricted to plane*, *sphere*)
3	saves the transformation being correct in a file and store it on the computer disk
4	updates the map in the Map viewer with the current alignment between each pair of scans
5	performs the ICP algorithm over the pair of scans presented on the viewer
6	does undo to the transformation computed with ICP

The information of each point cloud (color+geometric) is stored in text files on the computer memory disk. The PLY (Polygon) file format is used to store the information. The name of each file contains an ID, which represents the node of the graph where the scan is stored (e.g. *cloud_1.ply* means that cloud 1 is stored in node 1). The homogeneous transformation that align each pair of scans is also stored in the memory disk using text files (TXT format). The name of each transformation file contains two IDs corresponding to the scans that transformation aligns (e.g. *trans_1_2.txt* means that the transformation stored in this file aligns scan 2 with scan 1).

C

User Study Results

Table C.1: Results of the user performance in the 2D user study

User	Trial order	Trial	Time	Cost
1	1	Without Forces	8.57	48.87
	2	With Forces	8.37	29.76
2	1	Without Forces	11.48	41.29
	2	With Forces	6.77	30.90
3	1	Without Forces	15.97	47.79
	2	With Forces	11.43	35.46
4	1	Without Forces	18.15	31.29
	2	With Forces	12.52	26.90
5	2	Without Forces	14.58	32.12
	1	With Forces	8.50	32.26
6	2	Without Forces	15.07	31.52
	1	With Forces	14.70	27.03
7	2	Without Forces	19.80	34.43
	1	With Forces	10.10	34.65
8	2	Without Forces	26.53	27.54
	1	With Forces	13.52	27.82

Table C.2: Results of the user performance in the 3D user study

User	Experiment	Experiment order	Trial	Trial order	Time	Cost
1	Unrestricted Rotations	2	Without Forces	2	8m 43s	32288.76
			With Forces	1	5m 36s	31612.26
	Restricted Rotations	1	Without Forces	1	18m 51s	33117.41
			With Forces	2	7m 25s	32496.63
2	General Rotations	2	Without Forces	2	23m 01s	32302.85
			With Forces	1	11m 14s	31554.94
	Restricted Rotations	1	Without Forces	1	11m 09s	31821.65
			With Forces	2	11m 15s	32059.46
3	Unrestricted Rotations	2	Without Forces	2	6m 44s	33411.04
			With Forces	1	3m 22s	31762.60
	Restricted Rotations	1	Without Forces	1	5m 12s	32572.74
			With Forces	2	4m 23s	31175.23
4	Unrestricted Rotations	2	Without Forces	1	3m 35s	32328.11
			With Forces	2	2m 14s	32489.22
	Restricted Rotations	1	Without Forces	2	2m 30s	37075.51
			With Forces	1	5m 15s	32070.84
5	Unrestricted Rotations	2	Without Forces	1	3m 10s	31769.02
			With Forces	2	4m 15s	30679.01
	Restricted Rotations	1	Without Forces	2	4m 28s	33299.34
			With Forces	1	5m 17s	32334.10
6	Unrestricted Rotations	2	Without Forces	1	14m 06s	32400.59
			With Forces	2	10m 05s	31867.00
	Restricted Rotations	1	Without Forces	2	13m 24s	31472.45
			With Forces	1	13m 17s	32085.55
7	Unrestricted Rotations	1	Without Forces	2	4m 17s	33403.97
			With Forces	1	4m 41s	33011.99
	Restricted Rotations	2	Without Forces	1	3m 28s	31540.29
			With Forces	2	2m 30s	33227.85
8	Unrestricted Rotations	1	Without Forces	2	10m 22s	32077.07
			With Forces	1	11m 35s	30765.16
	Restricted Rotations	2	Without Forces	1	9m 55s	32734.47
			With Forces	2	10m 34s	32146.93
9	Unrestricted Rotations	1	Without Forces	2	6m 18s	32720.38
			With Forces	1	12m 19s	31501.42
	Restricted Rotations	2	Without Forces	1	6m 22s	32678.63
			With Forces	2	5m 20s	32113.42
10	Unrestricted Rotations	1	Without Forces	1	11m 17s	33494.21
			With Forces	2	7m 20s	31394.14
	Restricted Rotations	2	Without Forces	2	11m 17s	32904.15
			With Forces	1	6m 28s	32199.94
11	Unrestricted Rotations	1	Without Forces	1	24m 47s	32611.08
			With Forces	2	5m 09s	30973.78
	Restricted Rotations	2	Without Forces	2	6m 46s	32144.85
			With Forces	1	5m 54s	32220.62
12	Unrestricted Rotations	1	Without Forces	1	25m 23s	33827.35
			With Forces	2	9m 56s	31722.08
	Restricted Rotations	2	Without Forces	2	14m 40s	32488.70
			With Forces	1	12m 48s	32344.11